

Cite this: *Dalton Trans.*, 2024, **53**, 19179

Unravelling the potential of low-valent tunable vanadium complexes in the nitrogen reduction reaction (NRR)†

Bijoy Ghosh, Shtaz Ahmed and Ashwini K. Phukan *

Density functional theory calculations have been carried out to investigate the potential of several hitherto unknown low-valent tripodal vanadium complexes towards conversion of dinitrogen to ammonia as a function of different equatorial (P^iPr_2 and S^iPr) and bridgehead groups (B, C and Si). All the newly proposed vanadium complexes were probed towards understanding their efficiency in some of the key steps involved in the dinitrogen fixation process. They were found to be successful in preventing the release of hydrazine during the nitrogen reduction reaction. We have performed a comprehensive mechanistic study by considering all the possible pathways (distal, alternate and hybrid) to understand the efficiency of some of the proposed catalysts towards the dinitrogen reduction process. The exergonic reaction free energies obtained for some of the key steps and the presence of thermally surmountable barrier heights involved in the catalytic cycle indicate that these complexes may be considered as suitable platforms for the functionalization of dinitrogen.

Received 3rd August 2024,
Accepted 24th October 2024

DOI: 10.1039/d4dt02217c

rsc.li/dalton

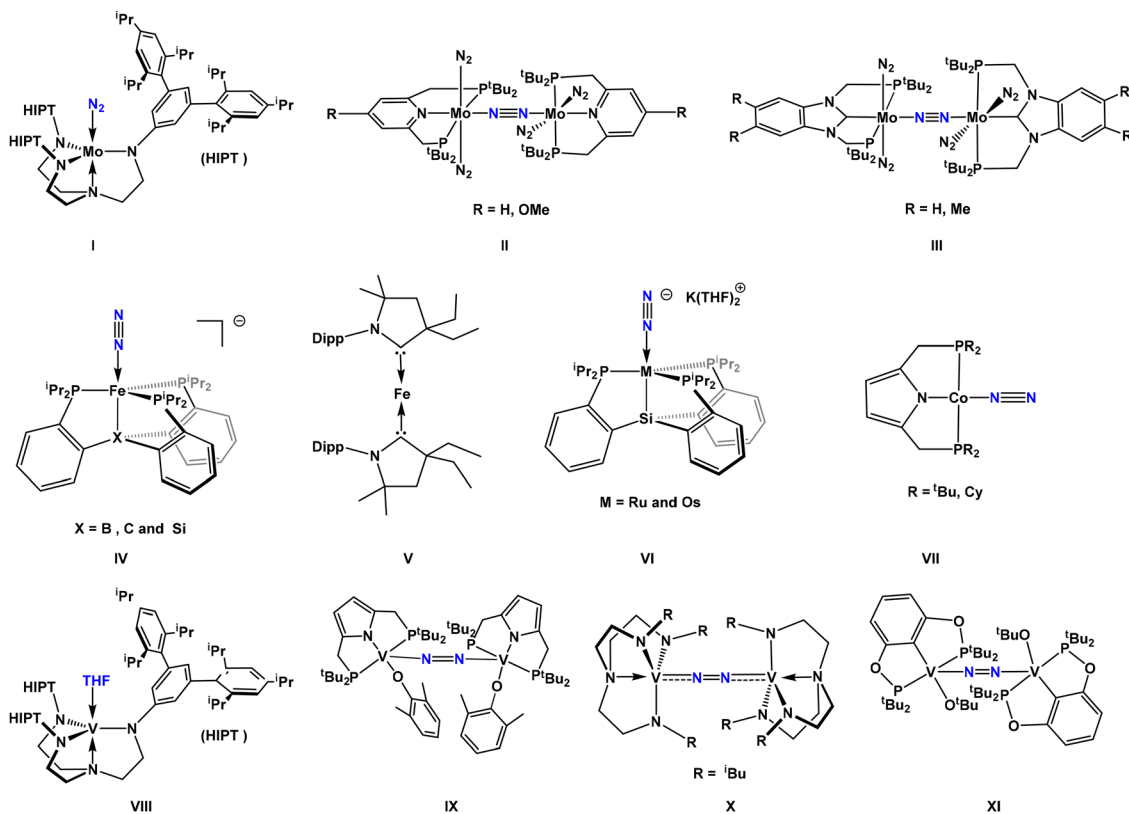
Introduction

The element nitrogen is essential for life on Earth. Although dinitrogen is one of the most available molecules surrounding us, its high thermodynamic stability (945 kJ mol^{-1})¹ and non-polar nature make it inert, and hence difficult to use in different chemical processes. Industrially, the best method known to date for the reduction of dinitrogen to ammonia is the Haber–Bosch process, which demands high temperatures (400–500 °C) and pressures ($\sim 200 \text{ atm}$).^{2,3} Interestingly, nature performs the conversion of N_2 to NH_3 under ambient conditions with the assistance of a group of enzymes known as nitrogenases, which contain transition metals (TM) such as Fe (iron-only nitrogenase), Mo (molybdenum nitrogenase) and V (vanadium nitrogenase) in their active sites.⁴ The enzyme nitrogenase contains two protein units – the larger one (Fe–Mo protein) consists of two P-clusters, which help in the electron transfer process, while the other unit contains two iron-molybdenum cofactors (FeMocos) where reduction of dinitrogen takes place.^{5,6} Therefore, efforts are being made to mimic the active sites of nitrogenase enzymes by developing suitable TM-based model systems that can carry out the reduction process under ambient conditions.^{7–10}

In 2003, Schrock and coworkers synthesized the first nitrogenase model system that can catalytically convert dinitrogen into ammonia¹¹ using a molybdenum complex (**I**, Scheme 1) that contains the sterically encumbered $[HIPTN_3N]^{3-}$ ligand, where $HIPT = 3,5-(2,4,6-iPr_3C_6H_2)_2C_6H_3$ (hexaisopropylterphenyl). Lutidinium [Lut] and decamethylchromocene were used as the proton source and reductant, respectively, and the overall yield was found to be 66%. In order to understand the mechanistic details of the N_2 reduction process, several intermediates were isolated and DFT calculations were performed.^{12–19} A few years later, in 2011, Nishibayashi and coworkers developed a dinuclear molybdenum dinitrogen complex (**II**) supported by a PNP pincer ligand that can produce up to 11.6 equivalents of NH_3 per molybdenum center by employing cobaltocene as a reductant and lutidinium triflate as a proton source.²⁰ Following this, they have reported a number of molybdenum-based pincer-type catalysts that can effectively convert dinitrogen to ammonia under mild reaction conditions.^{9,10} Furthermore, in 2017, the same group developed another dinuclear molybdenum system with N-heterocyclic carbene (NHC)-based PCP pincer ligands (**III**) that shows remarkable catalytic activity towards the reduction of dinitrogen to ammonia (230 equiv. of NH_3).²¹ The introduction of the carbene moiety into the PCP pincer ligand makes it not only a good σ donor but also a good π acceptor, which results in stronger interactions between the molybdenum center and the pincer ligand. Thus, the system can stabilize different reaction intermediates throughout the course of the reaction.

Department of Chemical Sciences, Tezpur University, Napaam 784028, Assam, India.
E-mail: ashwini@tezu.ernet.in

† Electronic supplementary information (ESI) available: Important tables, figures and cartesian coordinates. See DOI: <https://doi.org/10.1039/d4dt02217c>

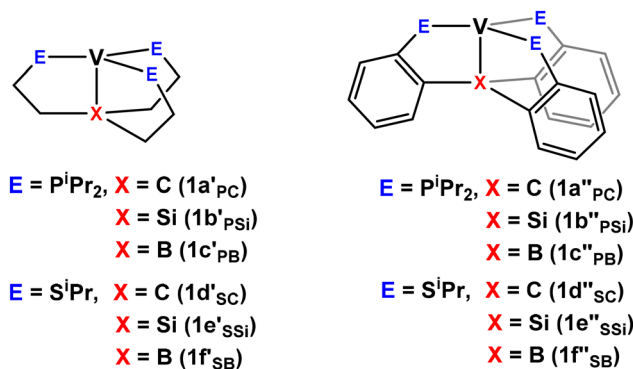


Scheme 1 Schematic representation of some synthetically amenable catalysts for nitrogen fixation.

Over the years, Peters and coworkers have synthesized and characterized a number of iron-based model systems (**IV**) that can mimic the biological activity of nitrogenase enzyme.^{22–25} Out of these model systems that have boron, carbon and silicon as the bridgehead atoms, the best results were obtained for the boron anchored example, which may be attributed to the flexibility of the Fe...B bond. The presence of a flexible Fe...B linkage allows the system to stabilize different intermediates (where Fe exists in various oxidation states) formed during the course of the reduction process, and results in better yields of ammonia (64 equiv. of NH₃).²⁶ The same group also synthesized a dicoordinate iron complex containing two CAAC (cyclic alkyl(amino)carbene) ligands which can not only bind dinitrogen but also reduce it to ammonia (4.7 equiv. NH₃) at low temperature (**V**).²⁷

Most of the model systems that have been designed to date contain iron or molybdenum as the central atom. However, a number of model systems with transition metals other than iron and molybdenum have also been reported.^{28,29} Peters and coworkers successfully synthesized tris(phosphine)silyl-ligand-supported osmium and ruthenium complexes (**VI**) that are capable of converting dinitrogen to ammonia under ambient pressure and at low temperatures.³⁰ Similarly, in 2016, Nishibayashi and coworkers reported the binding of dinitrogen to a cobalt PNP pincer complex (**VII**).³¹ In 2006, Schrock and coworkers successfully synthesized a vanadium analog of **I** (**VIII**),³² which, however, failed to produce ammonia under

similar reaction conditions. In a previous study, we had performed detailed computational investigations to understand the reasons behind the poor performance of **VIII** towards conversion of N₂ to NH₃.³³ The poor performance of the Schrock's vanadium complex (**VIII**) toward NH₃ production may be attributed to factors such as thermally unfavourable (*i.e.*, less exergonic) N–N bond cleavage and involvement of thermally unsurmountable barriers for protonation. In a ground-breaking study, Nishibayashi and coworkers reported the synthesis and isolation of the first vanadium-based catalyst (**IX**) that could catalytically convert N₂ to NH₃ under mild reaction conditions.³⁴ Kajita and coworkers synthesized a couple of dinitrogen-divanadium complexes (**X**) supported by triamidoamine ligands, which, upon reaction with the proton source (HOTf, HCl and [Lu]OTf) and reductant (M[C₁₀H₈], M = Na, K), led to the direct reduction of N₂ to NH₃ without generating hydrazine.^{35,36} Very recently, Hu and coworkers reported the synthesis of a divanadium pincer complex (**XI**) that can catalytically convert N₂ to NH₃ and N₂H₄.³⁷ It is pertinent to mention here that in terms of efficiency, the vanadium nitrogenase stands next to the molybdenum nitrogenase. However, only a limited number of vanadium-based complexes are known that can catalytically facilitate the conversion of dinitrogen to ammonia.³⁸ Therefore, there is not only ample scope but also a need to design and study a variety of biomimetic vanadium-based systems for the nitrogen reduction reaction (NRR). Herein, we present the results of a comprehensive com-



Scheme 2 Schematic representation of the model vanadium complexes considered in this study.

putational study on the potential of several low-valent tripodal vanadium complexes (Scheme 2) in the conversion of N₂ to NH₃, with special emphasis on some of the key steps involved in the NRR such as protonation of the metal–dinitrogen complex, formation of the metal nitride complexes *etc.* Our choice of the neutral tripodal system is prompted by the fact that the transition metal complex of such a ligand framework will have a higher d-electron count than that with an anionic ligand system such as the triamidoamine ligand present in the Schrock's vanadium complex **VIII**. For an easier identification of the complexes, the combination of the equatorial and bridgehead atoms was indicated by putting their respective symbols as subscripts. For example, [1a[']_{PC}] and [1a^{''}_{PC}] indicate the saturated and unsaturated complexes with phosphorus and carbon as the equatorial and bridgehead atoms, respectively. Furthermore, wherever possible, we have compared the energetics obtained for our proposed vanadium complexes with those of Schrock's vanadium complex ([HIPTN₃N]-V).³⁹

Computational details

Density functional theory (DFT) calculations were performed to optimize all the molecules without any symmetry constraints by employing the M06-L functional⁴⁰ in conjunction with the 6-311+G* basis set for all the elements.^{41–43} Our choice of the M06-L functional was prompted by previous reports of its suitability in not only reproducing experimental geometries but also in estimating or predicting the reaction energies of organometallic systems.^{44–52} We had verified this further by reproducing the experimentally observed geometrical parameters and IR wavelength for some synthetically achievable complexes^{32,34,37,53,54} (Fig. S1, ESI†). Frequency calculations were performed at the same level of theory to check the nature of the stationary points. All the ground-state structures were characterized by real frequencies while the transition states (TS) were characterized by the presence of only one imaginary frequency. The authenticities of the TSs were further probed by performing intrinsic reaction coordinate calculations (IRC) at the same level of theory. The polarized conti-

num model (PCM) was employed to include solvation effects for the solution-phase calculations using heptane as the solvent.⁵⁵ Since the energetics obtained for our proposed complexes were compared to that of Schrock's vanadium complex whose reactivity towards the NRR was investigated under similar reaction conditions that were successful for its molybdenum counterpart,¹¹ it may be sensible to use heptane as a solvent. Free energies corresponding to the protonation and reduction steps were evaluated relative to the processes LutH⁺ → Lut + H⁺ and [Cp*₂Cr] → [Cp*₂Cr]⁺ + e⁻, respectively, without any structural modification of the molecules involved (Cp*₂Cr = decamethyl chromocene and Lut = 2,6-dimethylpyridine). Dispersion effects were incorporated by using the D3 version of Grimme's dispersion correction coupled with the original D3 damping function with the keyword Empiricaldispersion = GD3.⁵⁶ The ultrafine grid was used throughout the calculations. Natural bonding orbital analysis was performed using the natural bond orbital (NBO)⁵⁷ scheme as implemented in the Gaussian 09 suite of programs.⁵⁸ In order to determine the activation energy barrier between species that have different ground-state multiplicities (spin states), the probable TSs were searched in all possible spin states, and the barrier height was computed by considering the lowest energy TS.^{59,60} Furthermore, since all the nitrogenous species involved in the catalytic cycle can exhibit more than one multiplicity, optimization of each species was performed by considering all the possible spin states, and the reaction free energies were calculated by considering the lowest-energy spin state. The energies of all the nitrogenous species in different spin states are listed in Tables S2, S4, S9, S13 and S20.† The energetics for all the calculations was evaluated in terms of changes in Gibbs free energies at 1 atm pressure and 298 K temperature, unless otherwise specified. Furthermore, we obtained negligible spin contaminations for all the complexes (Tables S3, S6 and S21†).

Furthermore, despite several attempts, we could not optimize the parent reduced species ([1a[']_{PC}]⁻–[1f[']_{SB}]⁻) at the M06-L-D3(heptane)/6-311+G* level. However, the same reduced species can be optimized at the M06-D3(heptane)/def2-SVP^{61–63} level of theory. Accordingly, the pathway C (Fig. 1)

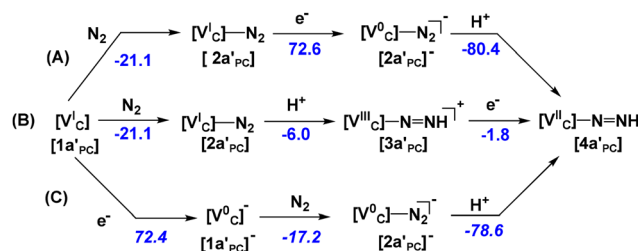
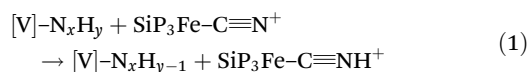


Fig. 1 The three possible pathways A, B and C for the conversion of [1a[']_{PC}] → [4a[']_{PC}]. The free energy values are in kcal mol⁻¹. The values given in *italics* were computed at the M06-L-D3(heptane)/6-311+G*//M06-D3(heptane)/def2-SVP level of theory. 2,6-Dimethylpyridine (Lut) and decamethyl chromocene (Cp*₂Cr) are considered as the protonation and reducing agents, respectively.

which is involved in the formation of the diazenido complex and the complete ligand exchange process (Fig. 11) were investigated by using the M06-L-D3(heptane)/6-311+G*/M06-D3(heptane)/def2-SVP level of theory. In order to verify the accuracy of the calculated (at M06-L functional) relative energy differences between the possible spin states, we re-evaluated some of these results by employing a few different functionals (PBE0-D3(heptane) and B3PW91-D3(heptane)).^{64,65}

Calculations of bond dissociation free energies (BDFEs)

The following hypothetical hydrogen atom transfer (HAT)⁵⁹ reaction has been employed to calculate the bond dissociation free energy (BDFE_{N-H}) of N-H bonds for some of the representative intermediates [V]-N_xH_y:



The reaction free energies for the HAT process were computed as:

$$\Delta G(\text{HAT}) = [G([\text{V}]-\text{N}_x\text{H}_{y-1}) + G(\text{SiP}_3\text{Fe}-\text{C}\equiv\text{NH}^+) - [G([\text{V}]-\text{N}_x\text{H}_y) + G(\text{SiP}_3\text{Fe}-\text{C}\equiv\text{N}^+)]$$

The BDFE_{N-H} of the complex **SiP₃Fe-C≡NH⁺** was experimentally determined (62 kcal mol⁻¹) in THF solution at 298 K and 1 atm⁶⁶ and, hence, is used as a reference complex for computing BDFE_{N-H} of the intermediates [V]-N_xH_y by employing the following equation:

$$\text{BDFE}_{\text{N-H}}([\text{V}]-\text{N}_x\text{H}_y) = \Delta G(\text{HAT}) + 62 \text{ kcal mol}^{-1}$$

In order to calculate the BDFE_{N-H}, we optimized a few representative vanadium nitrogenous species ([V]-N_xH_y) in the gas phase at the M06-L-D3/6-311+G* level of theory. The solvent effect (THF solvent in the PCM model) has been further incorporated by performing single-point calculations on M06-L-D3/6-311+G* optimized geometries to align with the experimental conditions (*i.e.*, in THF solution at 298 K and 1 atm). The Gibbs free energies (*G*) have been evaluated by adding the values of thermal correction to the Gibbs free energy acquired from the gas-phase frequency calculations with the solvent (THF)-corrected electronic energies.

Results and discussion

The process of dinitrogen reduction (NRR) facilitated by a transition metal catalyst is a complex, multi-step process and involves a large number of intermediates. As highlighted in the previous works, the formation of diazenido and nitride complexes, release of hydrazine and NH₃, addition of N₂, *etc.* are some of the elementary steps that generally occur during the NRR process.^{7,12-14,19b,32} Thus, before proceeding to study the entire NRR catalytic cycle, we decided to investigate the potential of the proposed catalysts in some of these elementary steps of the NRR as detailed below.

Formation of the diazenido complex

The optimized structures of the starting complexes [1a'_{PC}]-[1f'_{SB}] and [1a''_{PC}]-[1f''_{SB}] (Scheme 2) possess a trigonal monopyramidal geometry with the pyramidalization angle ($\theta = \circ - \sum \angle \text{E}-\text{V}-\text{E}$, E = S and P) at the vanadium center varying from 1.8 to 11.0° (Fig. S2 and Table S1†). Furthermore, in complexes with carbon or silicon as the bridgehead atoms, the vanadium center exhibits an oxidation state of +1 and hence they may give rise to three different spin states *viz.*, singlet, triplet and quintet states, with the quintet states being the most stable (the singlet and triplet states lie higher in energy by 13–33 kcal mol⁻¹ and 5–26 kcal mol⁻¹ respectively, Table S2†). Accordingly, we have considered only the quintet state geometry for the complexes with carbon and silicon as bridgehead groups in our study. Similarly, three different spin states, *viz.*, doublet, quartet and sextet states may be envisioned for vanadium complexes with boron as the bridgehead atom where the metal center exhibits an oxidation state of zero, and calculation of the relative energies of the spin state for [1c'_{PB}] reveals that the sextet state is the most stable one (the quartet and doublet states lie higher in energy by 11.4 and 23.4 kcal mol⁻¹, respectively). However, for [1f'_{SB}], the sextet and quartet states are isoenergetic (the energy difference between these states is only 1.3 kcal mol⁻¹); therefore, we have considered the sextet geometry for further study. However, the unsaturated vanadium complexes [1c''_{PB}] and [1f''_{SB}] compute the quartet state as their ground state. The important geometrical parameters of the vanadium complexes in their ground state are listed in Table S1.† Furthermore, we obtained negligible spin contaminations for the parent complexes in their different spin states (Table S3†).

Three different pathways, *viz.*, **A**, **B** and **C**, may be envisioned for the conversion of the bare complex (1) to the diazenido complex (4) as shown in Fig. 1 for the vanadium complex [1a'_{PC}] as a representative example. The first step for pathways **A** and **B** involves binding of N₂ to the bare complex [1a'_{PC}] producing [2a'_{PC}] ([V]^I-N₂). For complex [2a'_{PC}], three different spin states (singlet, triplet and quintet) are possible with the quintet state being the most stable (the singlet and triplet states are higher in energy by 27.7 and 8.7 kcal mol⁻¹, respectively, Table S4†). Hence, the quintet state of complex [2a'_{PC}] is considered for further study. The same is true for all the vanadium dinitrogen complexes considered in this study that feature carbon/silicon as the bridgehead atom (Table S4†). However, vanadium dinitrogen complexes with boron as the bridgehead atom ([2c'_{PB}], [2c''_{PB}], [2f'_{SB}] and [2f''_{SB}]) have the sextet state as their ground state. The calculated energies of the N₂ adduct of [1a'_{PC}]-[1f'_{SB}] and [1a''_{PC}]-[1f''_{SB}] in all possible spin states are listed in Table S4.† We obtained negligible spin contaminations for the dinitrogen vanadium complexes in their different spin states (Table S6†). Furthermore, it is to be noted that all the vanadium dinitrogen complexes exhibit a trigonal bipyramidal geometry (TBP) with the pyramidalization angle around the TM center ranging from 4.6 to 20.0° (Table S5†). Furthermore, MO analysis of [1a'_{PC}]-[1f'_{SB}],

$[1a''_{PC}]-[1f''_{SB}]$ and $\{[HIPTN_3N]-V\}$ reveals that all the bare vanadium complexes considered in this study exhibit substantially higher donicity ($E_{HOMO} = -2.0$ to -2.8 eV, Table S1†) compared to $\{[HIPTN_3N]-V\}$ ($E_{HOMO} = -4.1$ eV). In addition, the calculated natural charges at the TM center are found to be relatively more negative in $[1a'_{PC}]-[1f_{SB}]$ (0.024 to -0.375) and $[1a''_{PC}]-[1f''_{SB}]$ (0.024 to -0.383) compared to that in $\{[HIPTN_3N]-V\}$ (1.179) further corroborating the higher Lewis basicity of our proposed complexes (Table S1†). Therefore, in all the dinitrogen adducts of $[1a'_{PC}]-[1f_{SB}]$ and $[1a''_{PC}]-[1f''_{SB}]$, a higher degree of back donation from the filled metal orbitals to the antibonding molecular orbitals of dinitrogen ($V \rightarrow \pi^*_{N=N}$) can be expected. Indeed, the reaction $[1a'_{PC}] \rightarrow [2a'_{PC}]$ (Table 1) *i.e.* the binding of N_2 with $[1a'_{PC}]$ is found to be appreciably exergonic by -21.1 kcal mol $^{-1}$, whereas $\{[HIPTN_3N]-V\}$ shows only slightly exergonic (-1.2 kcal mol $^{-1}$) reaction free energy for the formation of $\{[HIPTN_3N]-V-N_2\}$ (Table 1). In addition, akin to $[1a'_{PC}]$, all newly proposed vanadium complexes ($[1b'_{PSi}]-[1f_{SB}]$ and $[1a''_{PC}]-[1f''_{SB}]$) have substantially exergonic reaction free energies (-10.0 to -23.0 kcal mol $^{-1}$, Table 1) for the formation of the dinitrogen adduct, thereby indicating their potential in N_2 binding. Furthermore, the $N \equiv N$ bond distances for the N_2 adducts of $[1a'_{PC}]-[1f_{SB}]$ and $[1a''_{PC}]-[1f''_{SB}]$ are computed to be somewhat longer (1.132–1.139 Å) and weaker (WBI = 2.491–2.559) than that in $\{[HIPTN_3N]-V-N_2\}$ (1.114 Å; WBI = 2.773) (Table S5†). Also, we observed a substantial lowering of the vibrational stretching frequency of N_2 in all the N_2 adducts of $[1a'_{PC}]-[1f_{SB}]$ and $[1a''_{PC}]-[1f''_{SB}]$ ($\nu_{NN} = 2003.1$ – 2060.7 cm $^{-1}$, Table S5†) compared to that in the free dinitrogen (2412.3 cm $^{-1}$, calculated at the same level of theory) and $\{[HIPTN_3N]-V-N_2\}$ complex (2229.6 cm $^{-1}$). The optimized geometry of a representative dinitrogen adduct ($[2c''_{PB}]$) along with its key frontier molecular orbitals are shown in Fig. 2. An analysis of these frontier orbitals reveals that the HOMO–4 corresponds to the donation of electron density from the metal to the vacant p orbital at boron, whereas the HOMO–2

and HOMO–3 show back-donation from the filled metal orbitals to the antibonding orbitals of N_2 .

Furthermore, to check the reliability of the calculated relative energy difference between the possible spin states of the complexes, we have recalculated them by using a few other functionals (PBE0 and B3PW91) by considering $[1d'_{SC}]-[1f_{SB}]$ and $[2d'_{SC}]-[2f_{SB}]$ as the representative complexes. The relative energy differences obtained employing these functionals are found to be comparable to those obtained using the M06-L level of theory, thereby lending credence to the level of theory used in this study (Table S7†).

It is to be noted that the metal–nitrogen (N_α) bonds ($V-N_\alpha$) in the saturated $[V]-N_2$ complexes were found to be somewhat stronger than those in the corresponding unsaturated analogs (Table S5†). For example, the calculated $V-N_\alpha$ bond in $[2b'_{PSi}]$ (WBI = 0.712) was computed to be relatively stronger than that in the unsaturated analog $[2b''_{PSi}]$ (WBI = 0.641). Such strengthening of the $V-N_\alpha$ bonds in the saturated dinitrogen complexes may be attributed to the relatively high Lewis basicity of $[1a'_{PC}]-[1f_{SB}]$ (Table S1†), which in turn facilitates enhanced backdonation from the metal center to the $\pi^*_{N=N}$ orbital. This is also reflected in the significant lowering of the $N \equiv N$ stretching frequency in the saturated dinitrogen complexes ($[2a'_{PC}]-[2f_{SB}]$) compared to that in their unsaturated analogs ($[2a''_{PC}]-[2f''_{SB}]$) (Table S5†). In addition, $[1a'_{PC}]-[1f_{SB}]$ show relatively more exergonic reaction free energies for the binding of dinitrogen compared to $[1a''_{PC}]-[1f''_{SB}]$ (Table 1). The second step in pathway A *i.e.*, reduction of $[2a'_{PC}]$ to $[2a'_{PC}]^-$ is hugely endergonic in nature ($+72.6$ kcal mol $^{-1}$) whereas the second step in pathway B, *i.e.*, protonation of $[2a'_{PC}]$ to generate $[3a'_{PC}]$ ($[V^{III}]-N=NH^+$) is slightly exergonic in nature (-6.0 kcal mol $^{-1}$). It is important to mention here that we have used 2,6-dimethylpyridine (Lut) and decamethyl chromocene (Cp^*_2Cr) as the protonation and reducing agents, respectively. The final steps for pathway A (protonation of complex $[2a'_{PC}]^-$) and pathway B (reduction of $[3a'_{PC}]$) are exergonic by -80.4 kcal mol $^{-1}$ and -1.8 kcal mol $^{-1}$, respect-

Table 1 Calculated (PCM(heptane)-M06-L-D3/6-311+G*) reaction free energies (in kcal mol $^{-1}$) for the different steps involved in the formation of the diazenido complex (4) from the bare complex (1) via three different pathways *viz.*, A, B and C. The values given in italics are computed at the M06-L-D3(heptane)/6-311+G**/M06-D3(heptane)/def2-SVP level of theory^a

Molecules	1→2	2→2 ⁻	2 ⁻ →4	2→3	3→4	1→1 ⁻	1 ⁻ →2 ⁻
a'_{PC}	-21.1	72.6	-80.4 (-78.6)	-6.0	-1.8	72.4	-17.2
b'_{PSi}	-23.0	59.7	-71.5 (-72.2)	-3.9	-7.9	63.3	-27.6
c'_{PB}	-23.0	73.7	-78.8 (-77.7)	-0.7	-4.4	76.8	-24.9
d'_{SC}	-22.1	72.7	-77.7 (-77.9)	0.4	-5.4	72.8	-23.7
e'_{SSI}	-22.3	66.5	-72.1 (-71.1)	-1.6	-4.0	58.1	-28.6
f'_{SB}	-22.2	64.3	-68.3 (-69.3)	0.2	-4.2	68.0	-25.8
a''_{PC}	-20.4	65.1	-70.2 (-70.0)	0.7	-5.8	64.7	-18.1
b''_{PSi}	-18.0	63.6	-68.1 (-63.5)	3.2	-7.8	64.3	-26.5
c''_{PB}	-12.6	45.0	-51.7 (-51.2)	5.5	-12.2	50.9	-21.9
d''_{SC}	-18.7	64.2	-66.6 (-65.3)	6.7	-9.2	65.1	-20.5
e''_{SSI}	-22.0	60.8	-65.4 (-64.5)	8.3	-12.9	67.9	-27.8
f''_{SB}	-10.0	50.1	-52.6 (-51.6)	8.7	-11.1	52.4	-23.8

^a Despite several attempts, we could not optimize the parent reduced species $[V]^-$ at M06-L-D3(heptane)/6-311+G*. However, the same reduced species can be optimized at the M06-D3(heptane)/def2-SVP level of theory. Accordingly, the complete pathway C was investigated by using the M06-L-D3(heptane)/6-311+G**/M06-D3(heptane)/def2-SVP level of theory.

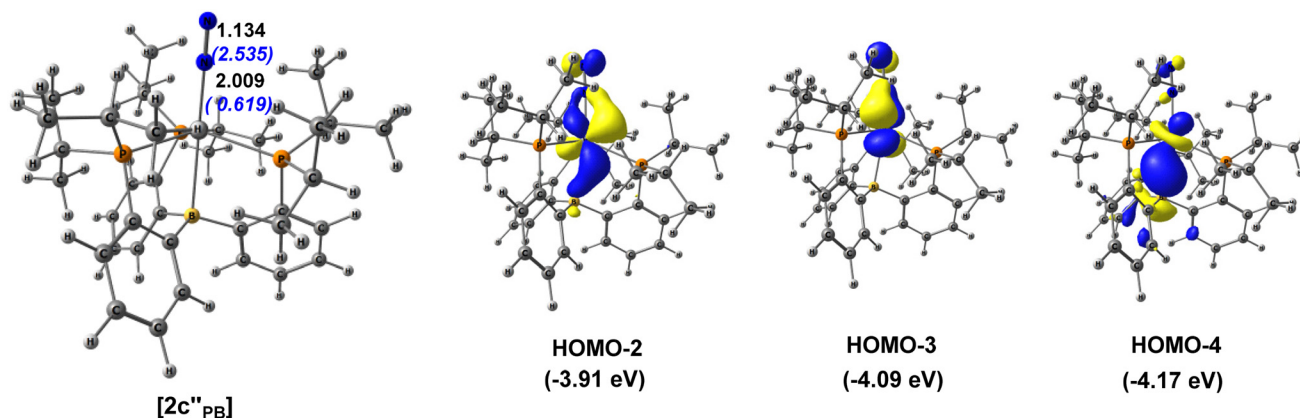


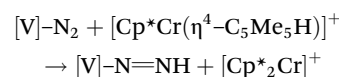
Fig. 2 Optimized geometry of a representative dinitrogen complex [2c''_{PB}] along with its important molecular orbitals. The bond lengths are in Å and WBI values are given within parentheses. The hydrogen atoms are omitted for the sake of clarity.

ively. In contrast, the first step in pathway C *i.e.*, reduction of the bare complex [1a'_{PC}] is highly endergonic in nature (72.4 kcal mol⁻¹), thus making it the least possible pathway. The next step in pathway C *i.e.*, addition of dinitrogen to [1a'_{PC}]⁻ is exergonic in nature (-17.2 kcal mol⁻¹) resulting in complex [2a'_{PC}]⁻ which is followed by a highly exergonic (-78.6 kcal mol⁻¹) protonation step producing [4a'_{PC}]. As a whole, the final species for all the pathways is complex [4a'_{PC}] ([V^{III}]-N=NH). From the above discussion, it is clear that the vanadium complex [1a'_{PC}] should favor pathway B for the conversion of the bare complex [1a'_{PC}] to the neutral diazenido complex [4a'_{PC}]. The same is also true for all the other vanadium complexes considered in this study (Table 1), considering Lut and Cp*₂Cr as the protonation and reducing agents. This is in line with earlier computational studies that showed pathway B to be the viable route for converting the parent complex into the neutral diazenido complex.^{16,33,67}

Schrock and coworkers also reported the characterization of the complex {[HIPTN₃N]-VN₂}⁻.³² Therefore, it may be helpful to make a comparison between [2a'_{PC}]⁻-[2f'_{SB}]⁻ and [2a''_{PC}]⁻-[2f''_{SB}]⁻ with {[HIPTN₃N]-VN₂}⁻. We found that the vibrational stretching frequency of N₂ was considerably lower in all the anionic complexes [2a'_{PC}]⁻-[2f'_{SB}]⁻ and [2a''_{PC}]⁻-[2f''_{SB}]⁻ (ν_{NN} = 1849.4–1963.2 cm⁻¹) than that in {[HIPTN₃N]-VN₂}⁻ (2061.2 cm⁻¹ *ca.* at the same level of theory), indicating the higher activation potential of our proposed complexes.

In a joint experimental and computational study, Peters and coworkers suggest the viability of a metallocene-mediated proton-coupled electron transfer (PCET) pathway as an additional contributor to the previously reported electron transfer-proton transfer (ET-PT) and proton transfer-electron transfer (PT-ET) pathways.⁶⁸ Similarly, they have also suggested the possibility of such a PCET pathway for previously reported Fe and Mo catalysts that employed metallocenes as reductants during the N₂ activation process.^{11,20,69} Since in this study, we have used Cp*₂Cr as a reductant, we have also studied the viability of such a pathway during the formation of the diazenido complexes. Employing LutH⁺ as a proton source, the formation

of the PCET reagent, *i.e.* *endo*-[Cp*Cr(η⁴-C₅Me₅H)]⁺, is computed to be thermodynamically favorable (-5.9 kcal mol⁻¹). The reaction free energy associated with the formation of the first intermediate ([V]-N=NH) *via* the PCET pathway is evaluated by employing the following equation



The reaction free energies associated with the formation of the diazenido complex *via* the PCET pathway for our proposed complexes are computed to be either marginally exergonic or thermoneutral in nature (-5.9 to 3.5 kcal mol⁻¹, Table S8[†]), thereby indicating the possibility of such a pathway during the N₂ activation process.

One of the important steps in N₂ reduction chemistry is the initial protonation of the dinitrogen molecule that results in elongation of the N-N bond. For vanadium complexes with PⁱPr₂ as the equatorial group ([2a'_{PC}]-[2c'_{PB}] and [2a''_{PC}]-[2c''_{PB}]), protonation may occur either directly at the distal nitrogen atom (N_β) or at the vanadium atom as shown in Fig. 3 for complex [2a'_{PC}] as a representative example. The former takes place in the second step of pathway B forming the complex [3a'_{PC}]. Furthermore, for the nitrogenous species [3] with carbon and silicon as the bridgehead group, two spin states are possible (singlet and triplet) with the triplet state being more stable than the singlet ones by 7.0–18.8 kcal mol⁻¹ (Table S9[†]). Similarly, for complex [3] with boron as the bridgehead group, two different spin states were considered *viz.*, doublet and quartet states, with the latter being more stable (Table S9[†]). However, for [V]-N₂ complexes with SⁱPr as an equatorial group ([2d'_{SC}]-[2f'_{SB}] and [2d''_{SC}]-[2f''_{SB}]), protonation may take place not only at the TM center and N_β, but also at the equatorial sulfur atom. Therefore, in the present study, we have considered all three possibilities for [2d'_{SC}]-[2f'_{SB}] and [2d''_{SC}]-[2f''_{SB}]. However, the reaction free energies obtained for protonation at the equatorial sulfur atom of [2d'_{SC}]-[2f'_{SB}] and [2d''_{SC}]-[2f''_{SB}] were substantially endergonic (16.9–22.2 kcal

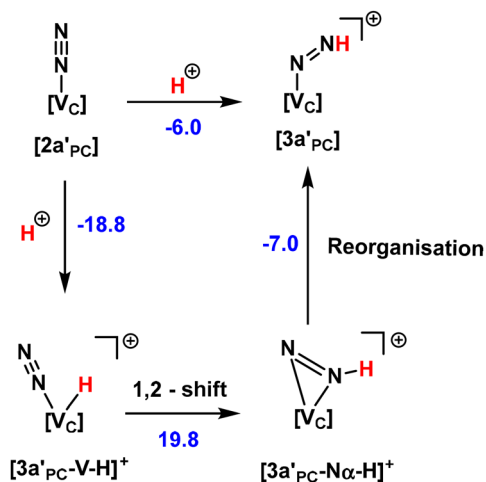


Fig. 3 Different possibilities for protonation of $[2a'_{PC}]$. Free energy values are in kcal mol⁻¹ calculated at the M06-L-D3(heptane)/6-311+G* level of theory. 2,6-Dimethylpyridine (Lut) is considered as the protonation agent.

mol⁻¹, Table S10,† see Fig. S3†), thereby ruling out such a possibility. Furthermore, the metal centers of $[2a'_{PC}]$ – $[2f'_{SB}]$ and $[2a''_{PC}]$ – $[2f''_{SB}]$ are highly basic in nature, which is not only evident from the calculated natural charges (Table S5†) but also from the fact that the HOMO is localized at vanadium (Fig. S4†). In agreement with this observation, direct protonation at the metal center is found to be considerably more exergonic (–18.8 kcal mol⁻¹) than protonation at the distal nitrogen (N_β) atom (–6.0 kcal mol⁻¹) as shown in Fig. 3. A similar

trend is observed for all other vanadium complexes proposed in this study (Table S10†). However, in order to activate the N–N bond, the proton has to bind to the distal nitrogen atom, thereby generating $[3]$. Accordingly, we searched for the possible pathway for the conversion of $[3a'_{PC-V-H}]^+$ to $[3]$. As shown in Fig. 3, the metal-protonated species $[3a'_{PC-V-H}]^+$ first undergoes a 1,2-proton shift to generate the η^2 -type intermediate $[3a'_{PC-N\alpha-H}]^+$, which then undergoes reorganization, generating $[3a'_{PC}]$ in its triplet ground state. The 1,2-shift process was considerably endergonic (19.8 kcal mol⁻¹) while the reorganization of $[3a'_{PC-N\alpha-H}]^+$ was exergonic by –7.0 kcal mol⁻¹. We have also calculated the activation energy barrier (ΔG^\ddagger) associated with the conversion of $[2a'_{PC}]$ to $[3a'_{PC}]$ via the intermediate $[3a'_{PC-N\alpha-H}]^+$ by locating the probable transition states (Fig. 4). The activation energy barriers associated with the 1,2-proton shift (+40.7 kcal mol⁻¹) and reorganization process (+16.7 kcal mol⁻¹) are quite high and hence, the metal protonated species $[3a'_{PC-V-H}]^+$ is unlikely to generate $[3a'_{PC}]$ ($[V^{III}]$ –N=NH⁺). The optimized geometries of the TSs (TS1 and TS2) and intermediate involved in the formation of $[2] \rightarrow [3]$ (via metal-protonated species) for all the vanadium complexes are shown in Fig. S5–S10,† and the energetics are listed in Table S11.† Similar to $[2a'_{PC}]$, the metal-protonated species of $[2b'_{PSi}]$ – $[2f'_{SB}]$ and $[2a''_{PC}]$ – $[2f''_{SB}]$ are not expected to produce complex $[3]$ because of the significantly higher barrier heights associated with their conversion (Table S11†). Therefore, it can be concluded that the most likely pathway for the generation of $[3]$ from $[2]$ is the direct protonation at the distal nitrogen atom. Following this, $[3a'_{PC}]$ undergoes reduction to form the neutral diazenido complex $[4a'_{PC}]$, in

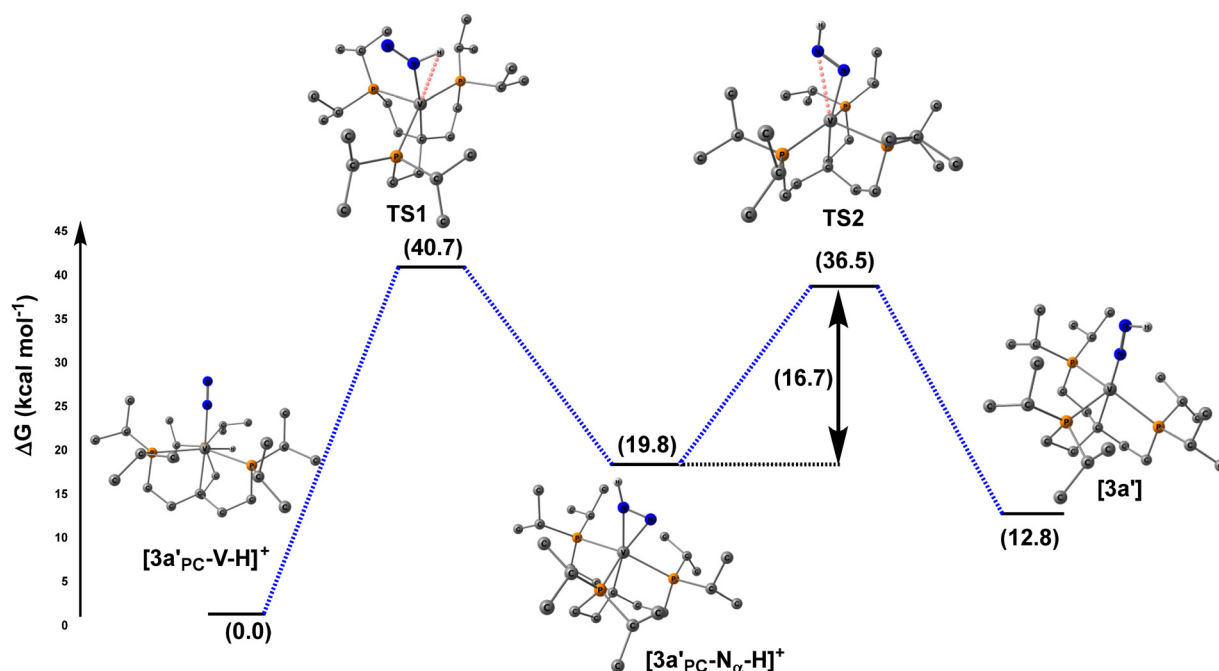


Fig. 4 Reaction profile diagram for the conversion $[3a'_{PC-V-H}]^+$ to $[3a'_{PC}]$ at the M06-L-D3(heptane)/6-311+G* level of theory. Hydrogen atoms of the methyl groups are omitted for clarity. The energy values are in kcal mol⁻¹.

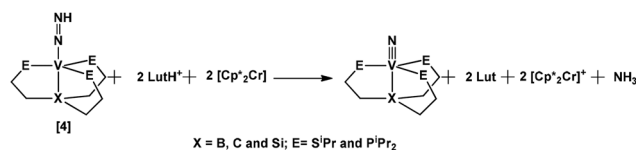
which the N–N bond is further activated, as is evident from the calculated N–N bond length (1.239 Å) and stretching frequency (1543.1 cm⁻¹, Table S12†). The diazenido complex [4] with carbon/silicon and boron as the bridgehead groups ([V_X]-N=NH; X = B, C, Si) has the quartet and quintet states as its ground states, respectively (Table S13†). Protonation at the distal nitrogen atom (N_β) not only activates the N–N bond but also induces polarity to the bond, as is evident from the calculated natural charges at both the nitrogen atoms of the diazenido complexes of [1a'PC]-[1f_{SB}] and [1a''PC]-[1f''SB] (Table S12†).

Furthermore, in an experimental study, Peters and co-workers reported the formation of a neutral hydride Fe–H–B complex for their iron catalyst.²³ Since protonation at the metal center for the complex [2c'_{PB}] is found to be exergonic in nature (–21.3 kcal mol⁻¹), we also studied the viability of the formation of such a neutral hydride V–H–B complex by considering [1c'_{PB}] as a representative case (Fig. 5). We could obtain one intermediate and a TS for the transformation of [2c'_{PB}-V-H]⁺ → [2c'_{PB}-V-H-B]. The reaction free energy associated with the formation of the intermediate [2c'_{PB}-V-H] *via* the reduction of [2c'_{PB}-V-H]⁺ is found to be exergonic in nature (–7.1 kcal mol⁻¹). Thereafter, [2c'_{PB}-V-H] reorganizes *via* a barrier-less process to yield the V–H–B complex. Therefore, the formation of such a neutral hydride species may also compete during the nitrogen reduction process for our proposed vanadium complexes.

Formation of the nitride complex

Another important step in the N₂ reduction chemistry is the protonation of the neutral diazenido complex (4), which

results in further elongation and polarization of the N–N bond. The protonation of the neutral diazenido complex may take place either at the N_β or N_α atom, leading to two different pathways *viz.*, alternating (or symmetric) and distal (or asymmetric) pathways.⁷⁰ In the alternating pathway, the protons are added alternately to the N_α and N_β atoms. On the other hand, in the distal pathway, the first three protons are consecutively added to the distal nitrogen atom, thereby generating the first equivalent of NH₃ and a nitride complex. Thereafter, the addition of the next three protons to the N_α atom produces the second equivalent of NH₃ along with the free catalyst. Therefore, in the distal pathway, the formation of the nitride complex is one of the most crucial steps, which not only breaks the N–N bond but also generates the first equivalent of NH₃.⁷¹ Accordingly, in order to further investigate the potential of the proposed tripodal vanadium complexes, we studied their efficiency towards the formation of the vanadium nitride complex by employing the following equation (Scheme 3). The calculated reaction free energies obtained for the generation of the vanadium nitride complex and the release of the first equivalent of ammonia from the respective diazenido complexes ([4]) were found to be substantially exergonic (–70.8 to –84.6 kcal mol⁻¹, Table S14†), thereby indicating their poten-



Scheme 3 Schematic representation of the reaction involved in the formation of vanadium nitride from the diazenido complex.

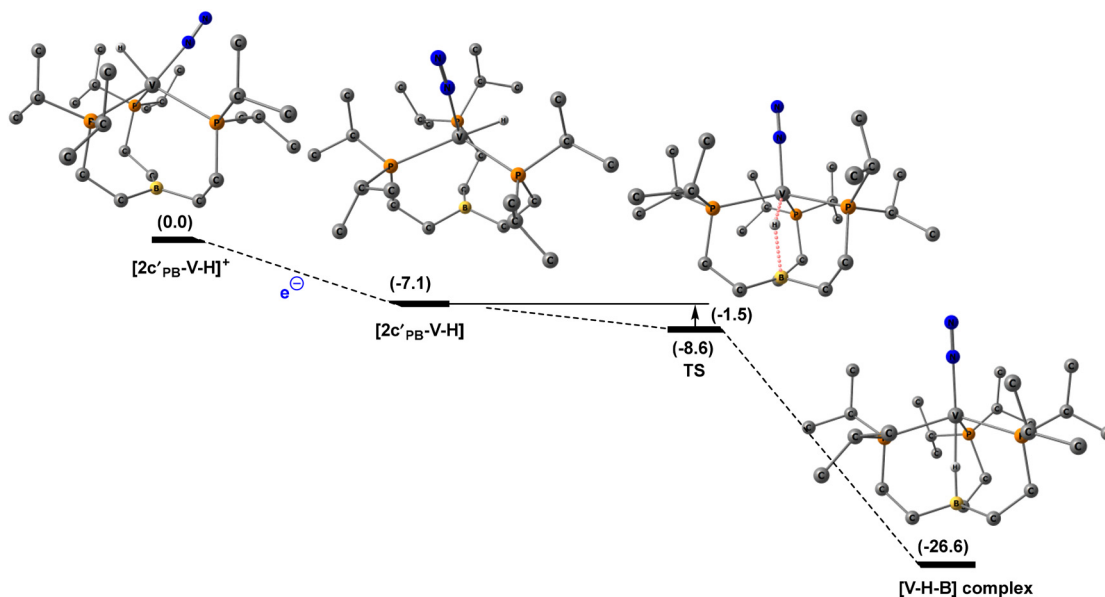


Fig. 5 Reaction profile diagram for the conversion of [2c'_{PB}-V-H]⁺ → [2c'_{PB}-V-H-B] complex at the M06-L-D3(heptane)/6-311+G* level of theory. Hydrogen atoms of the methyl groups are omitted for clarity. The energy values are in kcal mol⁻¹.

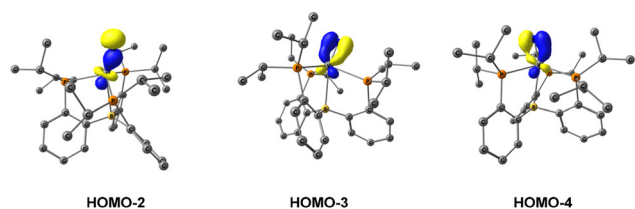
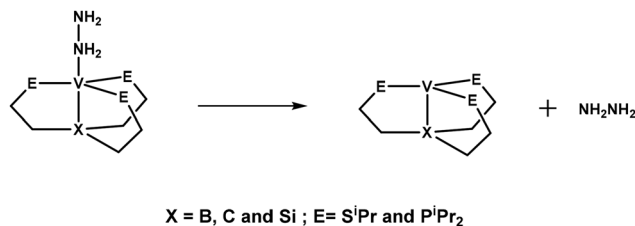


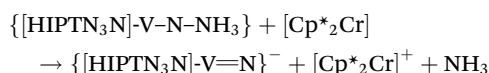
Fig. 6 Key frontier orbitals of the vanadium-nitride complex $[8c''_{PB}]_{dis}$ corresponding to the formation of one σ and two π bonds between vanadium and nitrogen. The hydrogen atoms of the methyl groups are omitted for clarity.



Scheme 4 Schematic representation of the reaction involved in the release of hydrazine from the vanadium-hydrazine complex.

tial toward the NRR. Furthermore, the calculated $V\equiv N$ bond lengths for the vanadium-nitride complexes lie within the range of 1.575–1.593 Å. In addition, the calculated WBI values (2.670–2.876, Table S15†) further corroborate the presence of a triple bond between vanadium and nitrogen. The key frontier molecular orbitals involved in the formation of the $V\equiv N$ bond for the vanadium-nitride complex of $[1c''_{PB}]$ ($[8c''_{PB}]_{dis}$) are shown in Fig. 6 as a representative example. An analysis of these frontier orbitals reveal that the HOMO-2 represents the formation of the σ -bond by the overlap of vanadium $3d_{z^2}$ with $2p_z$ of nitrogen, whereas the HOMO-3 (V $3d_{xz}/N 2p_x$) and HOMO-4 (V $3d_{yz}/N 2p_y$) correspond to the two π bonds between vanadium and nitrogen.

Furthermore, for the sake of comparison we have also studied the N–N bond breaking step for the Schrock's vanadium complex by employing the following reaction³³



The reaction free energy associated with the cleavage of the N–N bond and the generation of the first equivalent of NH_3 for Schrock's vanadium complex is found to be exergonic by $-16.8 \text{ kcal mol}^{-1}$ which is significantly lower than those obtained (Table S14†) for our proposed complexes. Therefore, it can be inferred that unlike $\{[HIPTN_3N]-V\}$ which failed to generate NH_3 , our proposed complexes may be considered as a suitable platform for the dinitrogen reduction process.

Release of hydrazine

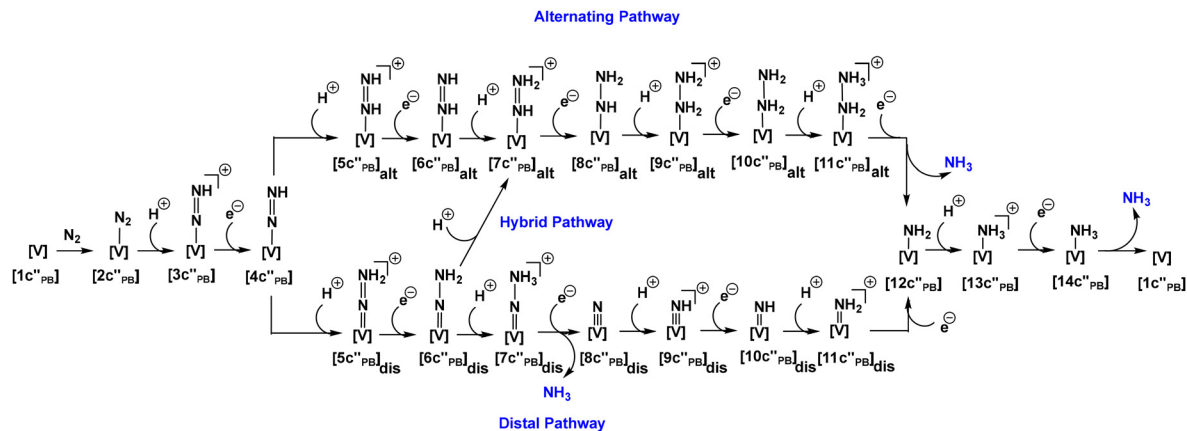
Another side reaction that competes during the nitrogen reduction process is the formation of hydrazine. For example, Peters and coworkers reported the formation of a trace amount of hydrazine upon treatment of their iron catalyst with the reductant and proton source.^{24,72} More recently, they have also shown that the iron hydrazido complex ($Fe=NNH_2$) – a key intermediate involved in the NRR – plays a selectivity-determining role towards generation of NH_3 and NH_2NH_2 .^{73,74} Similarly, some of the catalysts reported by Nishibayashi and coworkers also produce hydrazine as a side product during the NRR.^{34,75} However, our calculations suggest that the proposed vanadium complexes are unlikely to generate hydrazine

(Scheme 4) as a side product during the nitrogen reduction process, which is reflected in the endergonicity (11.2 to $17.7 \text{ kcal mol}^{-1}$, Table S16†) associated with the release of hydrazine from the vanadium-hydrazine complexes. Furthermore, the reaction free energy associated with release of hydrazine from Schrock's vanadium complex ($\{[HIPTN_3N]-V\}$) is also endergonic in nature ($9.7 \text{ kcal mol}^{-1}$) which perhaps explains why no hydrazine was detected upon treatment of the complex $\{[HIPTN_3N]-V\}$ with the proton source and reductant.

Furthermore, it is to be noted that all the complexes under consideration have almost similar energetics for the key steps of the NRR studied so far. The energetics computed for different steps employing B/C/Si as the bridgehead atom deviate from each other by less than 10 kcal mol^{-1} (Table 1 and Tables S14, S16†). Therefore, we decided to study the full catalytic cycle by considering boron anchored complexes $[1c''_{PB}]$ and $[1f''_{SB}]$ as representative examples. The motivation for choosing boron as the bridgehead group came from the experimental works of Peters and coworkers, who have reported higher activity of the boron-containing iron catalyst in the dinitrogen reduction process.^{23,76,77}

Nitrogen reduction reaction (NRR) with $[1c''_{PB}]$

As discussed above, the catalyst $[1c''_{PB}]$ favors the generation of the diazenido complex $[4c''_{PB}]$ ($[V]-N=NH$) (Table 1). The complex $[4c''_{PB}]$ thus formed is susceptible to further protonation as it features two lone pairs of electrons localized at the N_α and N_β atoms. Protonation at N_α or N_β atoms of $[4c''_{PB}]$ generates the cationic complexes $[5c''_{PB}]_{alt}$ ($[V]-NH=NH^+$) (in a quintet ground state) and $[5c''_{PB}]_{dis}$ ($[V]=N=NH_2^+$, in a triplet ground state), respectively, thereby bifurcating the catalytic cycle into two different pathways *viz.*, alternating and distal pathways (Scheme 5 and Fig. 7). The reaction free energies obtained for the formation of the nitrogenous species $[5c''_{PB}]_{alt}$ and $[5c''_{PB}]_{dis}$ are computed to be -9.8 and $-20.6 \text{ kcal mol}^{-1}$, respectively (Fig. 7). Therefore, from the thermodynamic point of view, it may be inferred that for the catalyst $[1c''_{PB}]$, the distal pathway may be preferred over the alternating pathway. In addition, we also looked for the probable TSs and intermediates involved in this transformation process. For the alter-



Scheme 5 Alternating, hybrid and distal pathways for dinitrogen reduction to NH_3 .

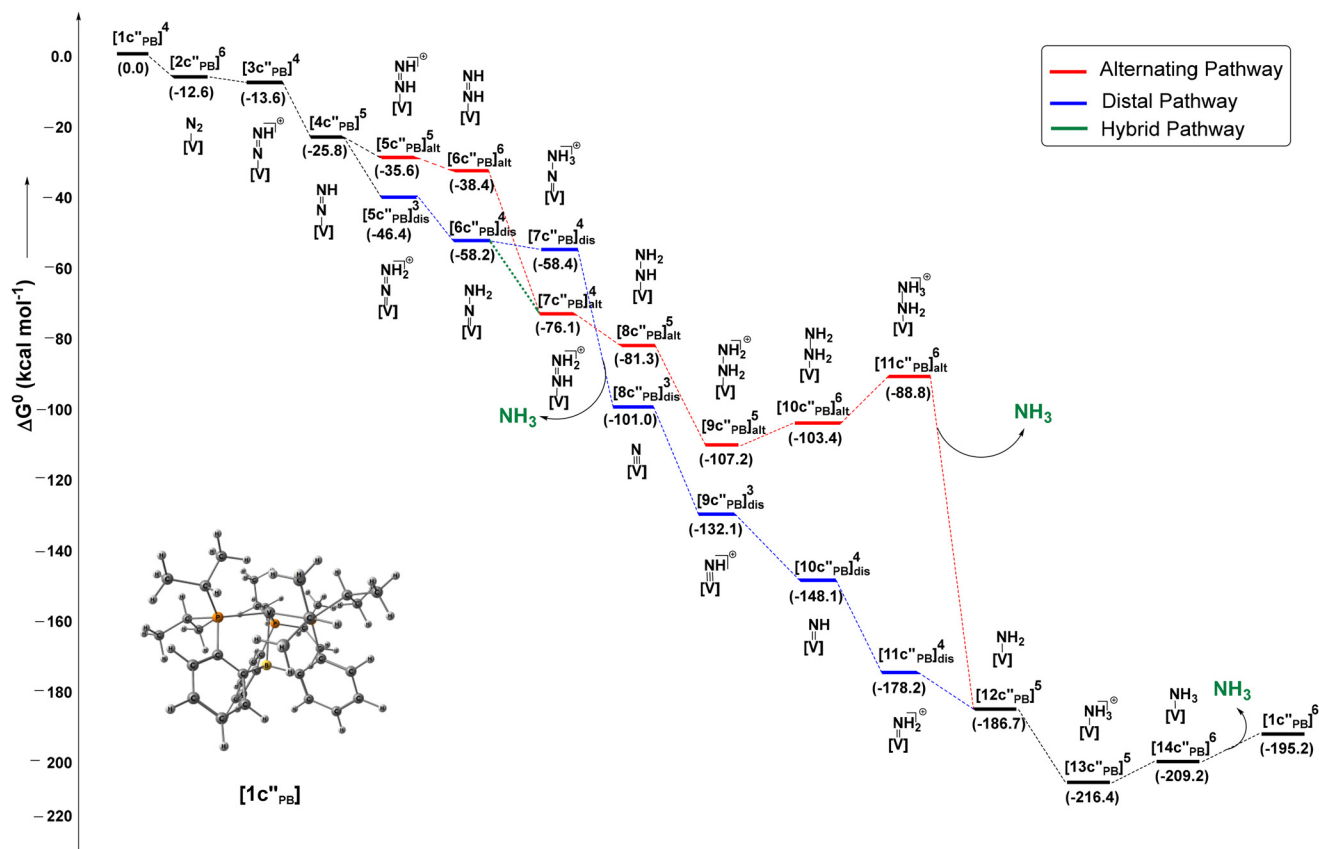


Fig. 7 Energy profile diagram for the reduction process of N_2 to NH_3 mediated by the catalyst $[1c''_{\text{PB}}]$. The energy values are given in kcal mol^{-1} and calculated at the M06-L-D3(heptane)/6-311+G* level of theory. The superscript outside the bracket indicates the spin state of the species. 2,6-Dimethylpyridine (Lut) and decamethyl chromocene (Cp^*_2Cr) are considered as the protonation and reducing agents, respectively.

nating pathway, we could locate an intermediate that is formed upon protonation at the metal center (Fig. 8). The formation of this intermediate $[4c''_{\text{PB}}\text{-V-H}]^+$ was computed to be marginally exergonic ($-4.5 \text{ kcal mol}^{-1}$) indicating that this reaction may also compete during the catalytic cycle. The intermediate thus formed passes through a TS ($\text{TS}_{3\text{alt}}$) in which the proton attached to the vanadium center migrates to the N_α

atom to yield the cationic complex $[5c''_{\text{PB}}]_{\text{alt}}$. Since the metal protonated species $[4c''_{\text{PB}}\text{-V-H}]^+$ ($S = 1$) and the complex $[5c''_{\text{PB}}]_{\text{alt}}$ ($S = 2$) exhibit different ground state multiplicities, we located the TSs in both multiplicities (triplet and quintet), and the barrier height was computed by considering the lowest-energy TS (Fig. S11†). The activation barrier obtained (considering the triplet state TS) for this transformation

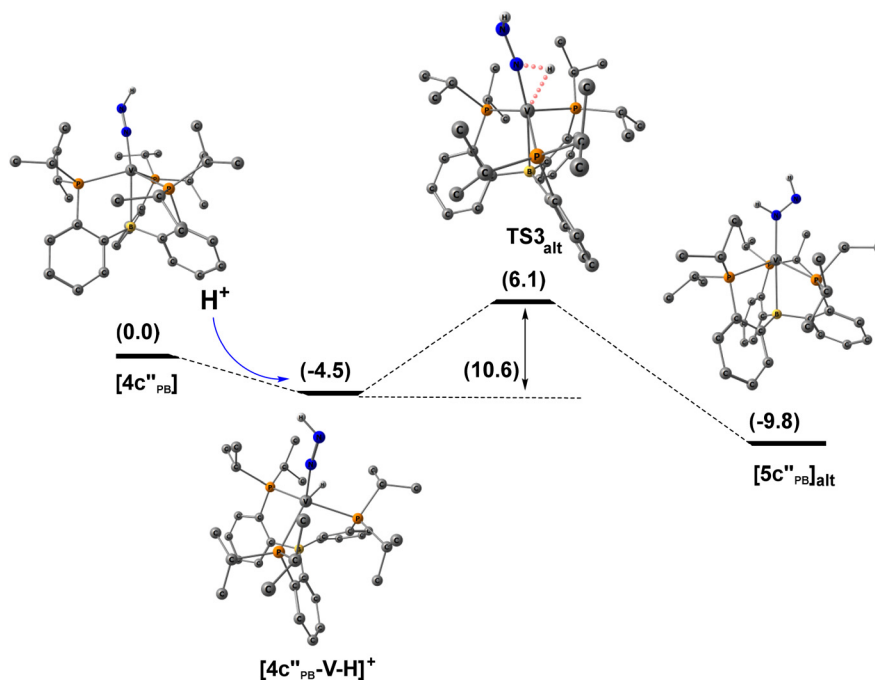


Fig. 8 Reaction profile diagram for the conversion of $[4c''_{PB}]$ to $[5c''_{PB}]_{alt}$ via an alternating pathway at the M06-L-D3(heptane)/6-311+G* level of theory. Hydrogen atoms of the methyl groups are omitted for clarity. The free energy values are in kcal mol⁻¹.

process ($[4c''_{PB-V-H}]^+ \rightarrow [5c''_{PB}]_{alt}$) was computed to be 10.6 kcal mol⁻¹. On the other hand, two intermediates and two TSs are involved in the conversion of $[4c''_{PB}] \rightarrow [5c''_{PB}]_{dis}$ via the distal pathway (Fig. 9).

The first step, *i.e.*, the formation of the metal protonated diazenido complex $[4c''_{PB-V-H}]^+$, is common for both pathways. Thereafter, $[4c''_{PB-V-H}]^+$ rearranges via a TS ($TS4'_{dis}$) to another η^2 -type intermediate ($\eta^2_{NN}[4c''_{PB-V-H}]^+$) with an acti-

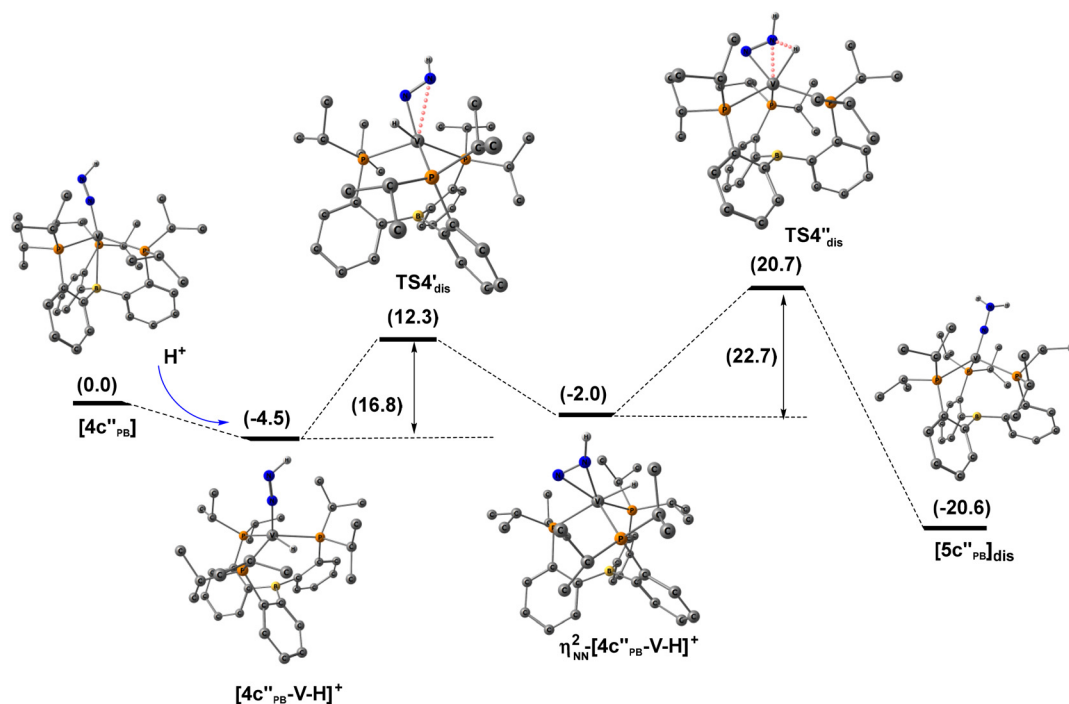


Fig. 9 Reaction profile diagram for the conversion of $[4c''_{PB}]$ to $[5c''_{PB}]_{dis}$ via a distal pathway at the M06-L-D3(heptane)/6-311+G* level of theory. Hydrogen atoms of the methyl groups are omitted for clarity. The free energy values are in kcal mol⁻¹.

vation barrier of 16.8 kcal mol⁻¹. Finally, $\eta^2_{\text{NN}}[4\text{c}''_{\text{PB}}\text{-V-H}]^+$ goes through another TS (TS4^{dis}) in which the proton attached to the metal center moves toward the distal nitrogen atom to generate $[5\text{c}''_{\text{PB}}]_{\text{dis}}$. The barrier height obtained for the process $\eta^2_{\text{NN}}[4\text{c}''_{\text{PB}}\text{-V-H}]^+ \rightarrow [5\text{c}''_{\text{PB}}]_{\text{dis}} ([\text{V}]=\text{N}=\text{NH}_2^{1+})$ is computed to be 22.7 kcal mol⁻¹. Therefore, from the kinetic point of view, both the pathways may be feasible, and depending upon the reaction conditions, one pathway may be favored over the other. Accordingly, we considered both pathways while studying the potential applicability of $[1\text{c}''_{\text{PB}}]$ in the dinitrogen reduction process.

Furthermore, it is to be noted that some of the nitrogenous species involved in the alternating and distal pathways are isomeric with one another (Scheme 5 and Fig. 7). For instance, species like $[5\text{c}''_{\text{PB}}]_{\text{alt}} ([\text{V}]\text{-NH}=\text{NH}^{1+})$, $[6\text{c}''_{\text{PB}}]_{\text{alt}} ([\text{V}]\text{-NH}=\text{NH})$ and $[7\text{c}''_{\text{PB}}]_{\text{alt}} ([\text{V}]\text{-NH}=\text{NH}_2^{1+})$, which we generally encounter in the alternating pathway are isomeric to the species $[5\text{c}''_{\text{PB}}]_{\text{dis}} ([\text{V}]=\text{N}=\text{NH}_2^{1+})$, $[6\text{c}''_{\text{PB}}]_{\text{dis}} ([\text{V}]=\text{N}=\text{NH}_2)$ and $[7\text{c}''_{\text{PB}}]_{\text{dis}} ([\text{V}]=\text{N}=\text{NH}_3^{1+})$, respectively, of the distal pathway. Hence, there is a possibility of interconversion of these species *via* either a proton-catalyzed (Fig. S12[†]) or a proton transfer (Fig. S13[†]) pathway. The calculated reaction free energies obtained for the deprotonation reactions involved in the conversion of these isomeric species *via* the proton-catalyzed pathway are computed to be considerably endergonic (9.8 to 19.4 kcal mol⁻¹) in nature, thereby ruling out the possibility of such an interconversion process. Similarly, we also located the probable TSs involved in the interconversion of these isomeric species *via* the proton transfer pathway. The barrier heights obtained for the processes $[5\text{c}''_{\text{PB}}]_{\text{alt}} ([\text{V}]\text{-NH}=\text{NH}^{1+}) \rightarrow [5\text{c}''_{\text{PB}}]_{\text{dis}} ([\text{V}]=\text{N}=\text{NH}_2^{1+})$, $[6\text{c}''_{\text{PB}}]_{\text{alt}} ([\text{V}]\text{-NH}=\text{NH}) \rightarrow [6\text{c}''_{\text{PB}}]_{\text{dis}} ([\text{V}]=\text{N}=\text{NH}_2)$ and $[7\text{c}''_{\text{PB}}]_{\text{alt}} ([\text{V}]\text{-NH}=\text{NH}_2^{1+}) \rightarrow [7\text{c}''_{\text{PB}}]_{\text{dis}} ([\text{V}]=\text{N}=\text{NH}_3^{1+})$ were substantially high (34.1–49.8 kcal mol⁻¹, Fig. S13[†]) indicating that such transformations are unlikely to take place. Furthermore, it is important to note that for the transformations $[5\text{c}''_{\text{PB}}]_{\text{alt}} \rightarrow [5\text{c}''_{\text{PB}}]_{\text{dis}}$ and $[6\text{c}''_{\text{PB}}]_{\text{alt}} \rightarrow [6\text{c}''_{\text{PB}}]_{\text{dis}}$, the starting reactant and the final species do not possess the same ground state multiplicity. Therefore, in order to obtain the activation energy barriers associated with these conversion processes, we have located the probable TSs in all the possible spin states, and the barrier heights were computed by considering the lowest energy TS (Fig. S14 and S15[†]).

In the alternating pathway, the species $[5\text{c}''_{\text{PB}}]_{\text{alt}} ([\text{V}]\text{-NH}=\text{NH}^{1+})$ which is formed upon protonation of the diazenido complex $[4\text{c}''_{\text{PB}}] ([\text{V}]\text{-N}=\text{NH})$ undergoes reduction to afford a neutral vanadium diazene complex $[6\text{c}''_{\text{PB}}]_{\text{alt}} ([\text{V}]\text{-NH}=\text{NH})$. The neutral complex $[6\text{c}''_{\text{PB}}]_{\text{alt}}$ can exhibit three different multiplicities *viz.*, sextet, quartet and doublet with the sextet state being the most stable one. Therefore, we considered the sextet geometry for free-energy calculations. The reaction process $[5\text{c}''_{\text{PB}}]_{\text{alt}} \rightarrow [6\text{c}''_{\text{PB}}]_{\text{alt}}$ is computed to be exergonic by -2.8 kcal mol⁻¹. The next step is the protonation of $[6\text{c}''_{\text{PB}}]_{\text{alt}}$ which generates a cationic complex $[7\text{c}''_{\text{PB}}]_{\text{alt}}$ in a quartet state, and this process is highly exergonic (-37.7 kcal mol⁻¹). Further reduction of $[7\text{c}''_{\text{PB}}]_{\text{alt}} ([\text{V}]\text{-NH}=\text{NH}_2^{1+})$, followed by the protonation of the resulting complex $[8\text{c}''_{\text{PB}}]_{\text{alt}} ([\text{V}]\text{-NH}=\text{NH}_2)$ in a

quintet ground state, generates a cationic vanadium(i) hydrazine complex $[9\text{c}''_{\text{PB}}]_{\text{alt}} ([\text{V}]\text{-NH}_2\text{-NH}_2^{1+})$ with no change in multiplicity. Both of these reaction processes *i.e.* conversion of $[7\text{c}''_{\text{PB}}]_{\text{alt}} ([\text{V}]\text{-NH}=\text{NH}_2^{1+}) \rightarrow [8\text{c}''_{\text{PB}}]_{\text{alt}} ([\text{V}]\text{-NH}=\text{NH}_2)$ and $[8\text{c}''_{\text{PB}}]_{\text{alt}} ([\text{V}]\text{-NH}=\text{NH}_2) \rightarrow [9\text{c}''_{\text{PB}}]_{\text{alt}} ([\text{V}]\text{-NH}_2\text{-NH}_2^{1+})$ were computed to be exergonic by -5.2 kcal mol⁻¹ and -25.9 kcal mol⁻¹, respectively. We observed a gradual elongation of the N–N bond length all the way from the species $[5\text{c}''_{\text{PB}}]_{\text{alt}}$ (1.278 Å) to $[9\text{c}''_{\text{PB}}]_{\text{alt}}$ (1.444 Å) (Table S17[†]), indicating the activation of the dinitrogen molecule. Reduction of $[9\text{c}''_{\text{PB}}]_{\text{alt}}$ requires 3.8 kcal mol⁻¹ to generate the neutral vanadium(0) hydrazine complex $[10\text{c}''_{\text{PB}}]_{\text{alt}} ([\text{V}]\text{-NH}_2\text{-NH}_2)$, with a sextet ground state. At this point of the catalytic cycle, the complex $[10\text{c}''_{\text{PB}}]_{\text{alt}}$ thus formed may either undergo further protonation or it can release hydrazine (N₂H₄) as a side product *via* the dissociation of the V–N_α bond. However, as mentioned earlier, the species $[10\text{c}''_{\text{PB}}]_{\text{alt}}$ shows a lower propensity to release N₂H₄, which is evident from the endergonicity associated with the release of N₂H₄ from the vanadium(0) hydrazine complex (14.8 kcal mol⁻¹, Table S16[†]). It should be noted that further protonation of $[10\text{c}''_{\text{PB}}]_{\text{alt}}$ also demands an energy of 14.6 kcal mol⁻¹ to yield the cationic complex $[11\text{c}''_{\text{PB}}]_{\text{alt}} ([\text{V}]\text{-NH}_2\text{-NH}_3^{1+})$ in a sextet ground state. The endergonicity associated with this protonation step may be traced to the energetically lower lying σ -donor orbital of the distal nitrogen atom ($E_{\text{LP}} = -6.7$ eV, Fig. S17[†]). However, the substantial exergonicity (-97.9 kcal mol⁻¹) of the next reduction step, *i.e.* the conversion of $[11\text{c}''_{\text{PB}}]_{\text{alt}} ([\text{V}]\text{-NH}_2\text{-NH}_3^{1+}) \rightarrow [12\text{c}''_{\text{PB}}] ([\text{V}]\text{-NH}_2)$ along with the release of the first equivalent of ammonia, may act as a driving force for the overall conversion of $[10\text{c}''_{\text{PB}}]_{\text{alt}}$ to $[12\text{c}''_{\text{PB}}]$ in a quintet ground state. Furthermore, it should be noted that the distal pathway is also a viable route for obtaining the vanadium(i) amide species $[12\text{c}''_{\text{PB}}] ([\text{V}]\text{-NH}_2)$. Therefore, both the pathways (alternating and distal) that bifurcated at $[4\text{c}''_{\text{PB}}] ([\text{V}]\text{-N}=\text{NH})$ again merge at this point. Such vanadium amide complexes ($[\text{V}]\text{-NH}_2$) are known experimentally,^{34,37} and are believed to be one of the key intermediates involved in the later stage of the dinitrogen reduction process.

As mentioned above, in the distal pathway, the protons are successively added to the distal nitrogen atom. In the first step of the distal pathway, the species $[5\text{c}''_{\text{PB}}]_{\text{dis}} ([\text{V}]=\text{N}=\text{NH}_2^{1+})$ that is formed upon protonation at the distal nitrogen atom of $[4\text{c}''_{\text{PB}}]$ undergoes reduction to generate a neutral hydrazido complex $[6\text{c}''_{\text{PB}}]_{\text{dis}} ([\text{V}]=\text{N}=\text{NH}_2)$ in a quartet ground state. The reaction free energy computed for this reduction process is -11.8 kcal mol⁻¹. The species $[6\text{c}''_{\text{PB}}]_{\text{dis}}$ bears two lone pairs of electrons and hence should undergo further protonation. Indeed, protonation of $[6\text{c}''_{\text{PB}}]_{\text{dis}}$ at the distal nitrogen atom generates a cationic species $[7\text{c}''_{\text{PB}}]_{\text{dis}} ([\text{V}]=\text{N}=\text{NH}_3^{1+})$ with a quartet ground state, and the process was computed to be thermoneutral in nature (-0.26 kcal mol⁻¹). The species $[7\text{c}''_{\text{PB}}]_{\text{dis}}$ features a substantially elongated N–N bond (1.407 Å), indicating considerable activation of the dinitrogen molecule (free N≡N bond length = 1.101 Å, *ca.* at the same level of theory). Reduction of $[7\text{c}''_{\text{PB}}]_{\text{dis}}$ led to splitting of the N–N bond, generating the first equivalent of NH₃ and a nitride

complex $[8c''_{PB}]_{dis}$ ($[V]\equiv N$) in a triplet ground state. This reduction step is computed to be highly exergonic in nature ($-42.8 \text{ kcal mol}^{-1}$). It is interesting to note that the reduction step that led to the generation of the first equivalent of NH_3 in the alternating pathway $[11c''_{PB}]_{alt}$ ($[V]-NH_2-NH_3^{1+}$) \rightarrow $[12c''_{PB}]$ ($[V]-NH_2$) is computed to be hugely exergonic (more than two times) compared to that *via* the distal pathway $[7c''_{PB}]_{dis}$ ($[V]=N-NH_3^{1+}$) \rightarrow $[8c''_{PB}]_{dis}$ ($[V]\equiv N$). The higher exergonicity associated with the release of the first equivalent of NH_3 in the alternating pathway ($-97.9 \text{ kcal mol}^{-1}$) may be attributed to the higher degree of activation of the N–N bond (1.469 Å, WBI = 0.772) in $[11c''_{PB}]_{alt}$ (N–N bond length in $[7c''_{PB}]_{dis}$: 1.407 Å; WBI: 1.018). $[8c''_{PB}]_{dis}$ features a triple bond between the vanadium and nitrogen atoms (V=N bond length in $[8c''_{PB}]_{dis}$: 1.580 Å; WBI: 2.713), and also a lone pair of electrons localized at the nitrogen atom (Fig. S18[†]). $[8c''_{PB}]_{dis}$ readily undergoes protonation, generating $[9c''_{PB}]_{dis}$ ($[V]\equiv NH^+$) without any change in the spin state, and this process is computed to be substantially exergonic by $-31.1 \text{ kcal mol}^{-1}$. Reduction of the species $[9c''_{PB}]_{dis}$ and the protonation of the ensuing complex $[10c''_{PB}]_{dis}$ ($[V]=NH$) in a quartet state generate the complex $[11c''_{PB}]_{dis}$ ($[V]=NH_2^{1+}$) with no change in multiplicity. These two reaction processes were computed to be considerably exergonic by -16.0 and $-30.1 \text{ kcal mol}^{-1}$, respectively. The next reduction step, *i.e.*, the conversion of $[11c''_{PB}]_{dis}$ to neutral vanadium(i) amide species $[12c''_{PB}]$, is exergonic as well ($-8.5 \text{ kcal mol}^{-1}$). NBO analysis suggests the presence of multiple bonds between vanadium and nitrogen in most of the nitrogenous species involved in the distal pathway (Table S17[†]). Furthermore, in an experimental study, Peters and coworkers demonstrated the viability of another pathway, *viz.*, a hybrid distal-to-alternating pathway, which may also operate during the nitrogen reduction process.⁶⁸ Indeed, the reaction free energy obtained for the transformation of $[6c''_{PB}]_{dis}$ ($[V]=N-NH_2$) \rightarrow $[7c''_{PB}]_{alt}$ ($[V]-NH=NH_2^{1+}$) is quite exergonic by $-18.0 \text{ kcal mol}^{-1}$, indicating that such a hybrid pathway may also be feasible during the nitrogen reduction process. We also studied the kinetics of this transformation ($[6c''_{PB}]_{dis} \rightarrow [7c''_{PB}]_{alt}$) by locating the probable intermediate and TS (Fig. 10). The first step involves the formation of a metal protonated species $[6c''_{PB}-V-H]^+_{dis}$ which is computed to be exergonic in nature ($-12.1 \text{ kcal mol}^{-1}$). Thereafter, $[6c''_{PB}-V-H]^+_{dis}$ passes through a TS (TS_{hyb}) with an activation barrier of $11.9 \text{ kcal mol}^{-1}$ to give $[7c''_{PB}]_{alt}$. Since the metal protonated species $[6c''_{PB}-V-H]^+_{dis}$ (doublet) and $[7c''_{PB}]_{alt}$ (quartet) exhibit different multiplicities, we attempted to locate the TS in both the spin states (doublet and quartet, Fig. S19[†]). It is found that the quartet state of TS_{hyb} is energetically more stable by $4.0 \text{ kcal mol}^{-1}$ than the corresponding doublet state (Fig. S19[†]). Therefore, the activation barrier was computed by considering the quartet state TS. Thus, thermodynamic and kinetic studies suggest the viability of the hybrid pathway in the NRR employing the catalyst $[1c''_{PB}]$.

The final three steps of the catalytic cycle are common for both pathways. Protonation of $[12c''_{PB}]$ affords a cationic complex $[13c''_{PB}]$ ($[V]-NH_3^{1+}$) in a quintet ground state (the

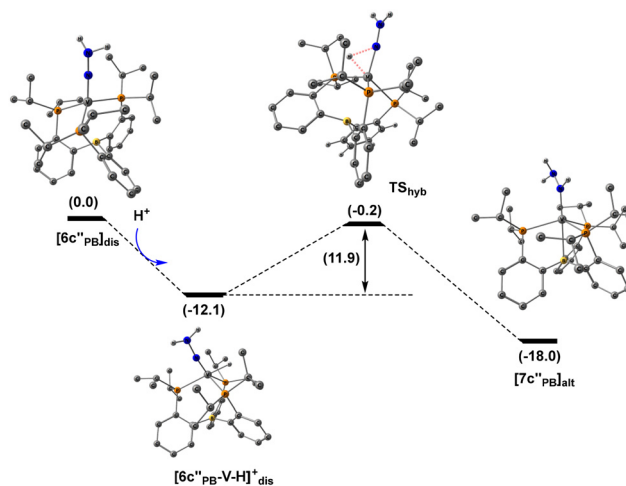
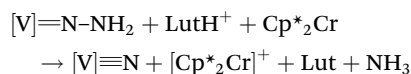


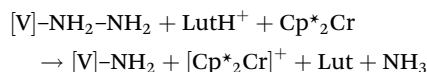
Fig. 10 Reaction profile diagram for the conversion of $[6c''_{PB}]_{dis} \rightarrow [7c''_{PB}]_{alt}$ *via* a hybrid pathway at the M06-L-D3(heptane)/6-311+G* level of theory. Hydrogen atoms of the methyl groups are omitted for clarity. The free energy values are in kcal mol^{-1} .

singlet and triplet states are higher in energy by 33.0 and $8.5 \text{ kcal mol}^{-1}$, respectively). This protonation process is calculated to be considerably exergonic by $-29.7 \text{ kcal mol}^{-1}$. However, reduction of $[13c''_{PB}]$ to generate $[14c''_{PB}]$ ($[V]-NH_3$) is calculated to be endergonic by $7.2 \text{ kcal mol}^{-1}$. The last step of the catalytic cycle is a key one, as it leads to the regeneration of the catalyst $[1c''_{PB}]$, and release of the second equivalent of ammonia. This process is computed to be endergonic by $14.0 \text{ kcal mol}^{-1}$. Similar energetics were also obtained for this last step, employing Schrock's molybdenum catalyst (**I**) by Reiher ($27.7 \text{ kcal mol}^{-1}$)¹⁶ and Tuzek ($8.8 \text{ kcal mol}^{-1}$).¹⁵ At this point of the catalytic cycle, $[1c''_{PB}]$ again needs to bind with dinitrogen to restart the nitrogen reduction process. Gratifyingly, the reaction free energy associated with the binding of N_2 with $[1c''_{PB}]$ is an exergonic process ($-19.1 \text{ kcal mol}^{-1}$, Table 1). Therefore, the overall NH_3 and N_2 exchange process for the catalyst $[1c''_{PB}]$ is computed to be exergonic by $-5.0 \text{ kcal mol}^{-1}$. Hence, from the above discussion, it can be inferred that the proposed vanadium catalyst $[1c''_{PB}]$ may be considered as a promising system for the nitrogen reduction reaction, which is not only evident from the highly exergonic calculated reaction free energies of different steps but also from the thermally surmountable, moderate barrier heights associated with these steps. To further support our findings, we also investigated the release of the first equivalent of NH_3 *via* both the distal and alternating pathways, taking into account the mononuclear form of the synthetically achievable Hu's vanadium complex **XI**.³⁷ To this end, we have computed its respective reaction free energies for both the distal and alternating pathways as shown below.

Distal



Alternate



It is encouraging to note that the reaction free energies computed for the release of the first equivalent of NH_3 by $[\mathbf{1c}''_{\text{PB}}]$ via distal ($-42.9 \text{ kcal mol}^{-1}$) and alternating ($-83.3 \text{ kcal mol}^{-1}$) pathways are found to be comparable to that obtained for Hu's vanadium catalyst **XI** (-52.1 and $-77.8 \text{ kcal mol}^{-1}$ for transformations via the distal and alternate pathways, respectively).

Furthermore, we also studied the full catalytic cycle by employing the catalyst $[\mathbf{1f}'_{\text{SB}}]$ (bearing S^iPr as the equatorial group). The energy profile diagram for the conversion of N_2 to NH_3 mediated by $[\mathbf{1f}'_{\text{SB}}]$ is given in Fig. S20† and the energetics was found to be comparable to that obtained using $[\mathbf{1c}''_{\text{PB}}]$. For example, release of the first equivalent of NH_3 along the distal and alternate pathways was calculated to be exergonic by -43.5 and $-97.2 \text{ kcal mol}^{-1}$, respectively, which are comparable to those obtained for $[\mathbf{1c}''_{\text{PB}}]$ (-42.8 and $-97.9 \text{ kcal mol}^{-1}$ respectively). Akin to the catalyst $[\mathbf{1c}''_{\text{PB}}]$, both thermodynamic and kinetic studies indicate the viability of the alternate and distal modes of protonation during the nitrogen reduction process for the catalyst $[\mathbf{1f}'_{\text{SB}}]$ (Fig. S21 and S22†). Similarly, the possibility of the interconversion of the isomeric species $[\mathbf{5f}'_{\text{SB}}]_{\text{alt}}$, $[\mathbf{6f}'_{\text{SB}}]_{\text{alt}}$ and $[\mathbf{7f}'_{\text{SB}}]_{\text{alt}}$ to $[\mathbf{5f}'_{\text{SB}}]_{\text{dis}}$, $[\mathbf{6f}'_{\text{SB}}]_{\text{dis}}$ and $[\mathbf{7f}'_{\text{SB}}]_{\text{dis}}$, respectively, may be ruled out from thermodynamic and kinetic studies (Fig. S13 and Fig. S24†). Furthermore, both thermodynamic and kinetic studies suggest the viability of the hybrid pathway for the catalyst $[\mathbf{1f}'_{\text{SB}}]$ (for details, please see Fig. S25† and the associated text). A major difference between the catalysts $[\mathbf{1f}'_{\text{SB}}]$ and $[\mathbf{1c}''_{\text{PB}}]$ is that in the case of $[\mathbf{1f}'_{\text{SB}}]$, the equatorial sulfur atom is susceptible to protonation during each phase of protonation. However, protonation at the sulfur atom for each protonation step is computed to be considerably endergonic (11.1 to $27.0 \text{ kcal mol}^{-1}$, Table S18†), thereby precluding such a possibility. Furthermore, similar to $[\mathbf{1c}''_{\text{PB}}]$, the reaction free energies obtained for different steps of the catalytic cycle by employing $[\mathbf{1f}'_{\text{SB}}]$ were found to be thermodynamically feasible, and also the barrier heights associated with the TSs are low, indicating its potential use as a catalyst for the dinitrogen reduction process.

Dissociation of NH_3 and addition of N_2

The ligand exchange process, which involves the dissociation of NH_3 and addition of N_2 , is one of the crucial steps in the dinitrogen reduction process that occurs at the end of the catalytic cycle. Both experimental¹³ and theoretical studies^{16,33} suggested that different routes, *viz.*, anionic, cationic and neutral pathways, are possible for the ligand exchange (N_2/NH_3) reaction (Fig. 11). Accordingly, all the different pathways were considered while investigating the efficiency of $[\mathbf{1c}''_{\text{PB}}]$ and $[\mathbf{1f}'_{\text{SB}}]$ towards the ligand exchange reaction. It is clear

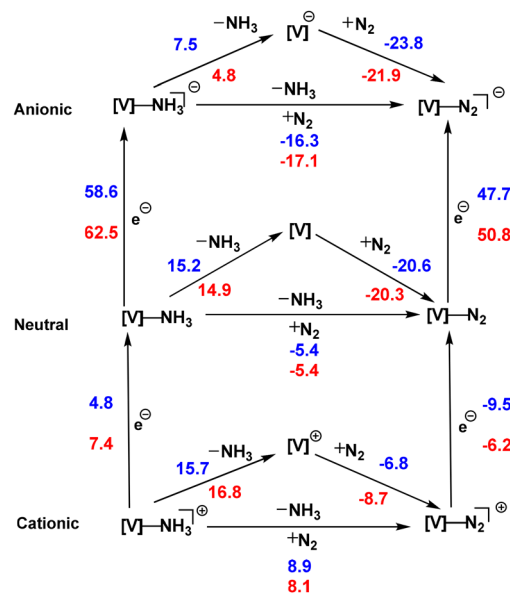


Fig. 11 Three different possibilities of NH_3/N_2 exchange. The energies are given in kcal mol^{-1} and calculated at the M06-L-D3(heptane)/6-311+G*/M06-D3(heptane)/def2-SVP level of theory. The free energy values given in blue and red colors correspond to the catalysts $[\mathbf{1c}''_{\text{PB}}]$ and $[\mathbf{1f}'_{\text{SB}}]$, respectively.

from Fig. 11 that for $[\mathbf{1c}''_{\text{PB}}]$ and $[\mathbf{1f}'_{\text{SB}}]$, the conversion of $[\text{V}]\text{-NH}_3^+$ to $[\text{V}]\text{-N}_2^+$ via the cationic pathway is thermodynamically unfavorable, which is reflected in the endergonicity associated with this exchange process. However, the other two exchange pathways, *viz.*, anionic and neutral, are thermodynamically viable. Furthermore, for all the pathways, the dissociation of the σ -donor NH_3 is a demanding process as reflected in the endergonic reaction free energies (4.8 to $16.8 \text{ kcal mol}^{-1}$). On the other hand, the addition of dinitrogen to the vanadium center is computed to be considerably exergonic (-6.8 to $-23.8 \text{ kcal mol}^{-1}$). Even though reduction of $[\text{V}]\text{-NH}_3^+ \rightarrow [\text{V}]\text{-NH}_3$ is not an energetically demanding process, the subsequent reduction of $[\text{V}]\text{-NH}_3$, which results in the formation of an anionic complex $[\text{V}]\text{-NH}_3^-$, is calculated to be highly endergonic (as shown in the left hand side of Fig. 11). Furthermore, the reduction processes $[\text{V}]\text{-N}_2^+ \rightarrow [\text{V}]\text{-N}_2$ and $[\text{V}]\text{-N}_2 \rightarrow [\text{V}]\text{-N}_2^-$ are computed to be moderately exergonic (-6.2 to $-9.5 \text{ kcal mol}^{-1}$) and highly endergonic (47.7 to $50.8 \text{ kcal mol}^{-1}$), respectively, in nature (as shown in the right hand side of Fig. 11). Therefore, unlike the molybdenum catalyst (**I**), which favors both anionic and neutral pathways,¹⁶ our calculations suggest that the proposed catalysts $[\mathbf{1c}''_{\text{PB}}]$ and $[\mathbf{1f}'_{\text{SB}}]$ should follow only the neutral pathway for the ligand exchange process.

Possibility of the hydrogen evolution reaction (HER)

Previous experimental studies indicate that the hydrogen evolution reaction (HER) is one of the undesirable side reactions

Table 2 Computed BDFE_{N-H} (in kcal mol⁻¹) of the N-H bond for some of the important intermediates ([V]-N_xH_y) formed during the NRR cycle. The ground state multiplicities of the intermediates are mentioned as superscripts

Intermediates	Chemical formula	BDFE _{N-H} (kcal mol ⁻¹)
[4c'' _{PB}] ⁵	[V]-N=NH	43.8
[6c'' _{PB}] ⁴ _{dis}	[V]=N-NH ₂	72.2
[6c'' _{PB}] ⁶ _{alt}	[V]-NH=NH	55.0
[7c'' _{PB}] ⁴ _{alt}	[V]-NH=NH ₂ ¹⁺	81.3
[8c'' _{PB}] ⁵ _{alt}	[V]-NH-NH ₂	72.7

that could compete with the NRR during the catalytic process.²⁴ It is to be noted that the higher degree of reactivity of the intermediates ([V]-N_xH_y), particularly those with weaker N-H bonds, may promote the unwanted HER. In a previous computational study, Oláh and co-workers predicted that nitrogenous species with BDFE_{N-H} values in the range of 41–62 kcal mol⁻¹ are prone to the HER while those above that range are unlikely to facilitate the HER.⁵⁹

Therefore, we decided to investigate whether these intermediates facilitate the NRR or the HER. To evaluate this, we assessed the N-H bond strength in terms of the computed BDFE_{N-H} (see computational details) of these intermediates as previous studies suggest that a higher N-H bond strength correlates with a reduced tendency for the HER.⁵⁹ We have selected the intermediates (Table 2) from different stages (early, moderate and late) of the catalytic process to explore how the N-H bond strength influences their potential for the HER *versus* NRR. It is encouraging to note that the computed BDFE_{N-H} values for some of the investigated intermediates were found to be significantly higher (Table 2) and hence may facilitate the NRR over the HER.

Conclusions

Quantum chemical (DFT) calculations have been carried out to study the potential of a series of tunable low-valent tripodal vanadium complexes as catalysts in the nitrogen reduction reaction (NRR). All our proposed complexes were found to be capable of dinitrogen functionalization as reflected in the thermodynamic feasibility of several key steps (binding of nitrogen, formation of the diazenido and nitride complex *etc.*) investigated in this study. For instance, the reaction free energies associated with the formation of N₂ adducts with [1a'_{PC}]-[1f'_{SB}] and [1a''_{PC}]-[1f''_{SB}] were found to be substantially exergonic in nature (-18.0 to -23.0 kcal mol⁻¹, considerably higher than that obtained for Schrock's system), thereby indicating their potential in dinitrogen binding. In addition, the exergonicity related to the formation of nitride complexes of [1a'_{PC}]-[1f'_{SB}] and [1a''_{PC}]-[1f''_{SB}] were found to be significantly higher than that of Schrock's vanadium complex, suggesting their superior potential towards the NRR. One of the major advantages of these proposed complexes is that they are unlikely to generate hydrazine during the NRR. In addition, we performed

a comprehensive mechanistic study to understand the efficiency of the catalysts [1c''_{PB}] and [1f''_{SB}] by considering all possible pathways *viz.*, alternating and distal pathways, and both thermodynamic and kinetic studies reveal the viability of these two pathways. Our calculations also suggest the possibility of the hybrid distal-to-alternating pathway that may operate during the nitrogen reduction process (as suggested by Peters and coworkers in an earlier report⁶⁸). In addition, our calculations rule out the possibility of interconversion of the isomeric nitrogenous species involved in the alternating [5c''_{PB}]_{alt} ([V]-NH=NH¹⁺), [6c''_{PB}]_{alt} ([V]-NH=NH) and [7c''_{PB}]_{alt} ([V]-NH=NH₂¹⁺), and distal [5c''_{PB}]_{dis} ([V]=N-NH₂¹⁺), [6c''_{PB}]_{dis} ([V]=N-NH₂) and [7c''_{PB}]_{dis} ([V]=N-NH₃¹⁺), pathways. Furthermore, there is also scope for protonation at the vanadium center, as indicated by the exergonicity associated with this process. Therefore, this reaction may also compete during the nitrogen reduction process. Furthermore, our calculations suggest that the proposed catalysts [1c''_{PB}] and [1f''_{SB}] should follow only the neutral pathway for the ligand exchange process. In addition, both the tripodal catalysts are likely to serve as potential candidates for the NRR, which is evident not only from the calculated highly exergonic reaction free energies of the different key steps but also from the moderate barrier heights associated with these transformations. The calculations demonstrate that the proposed neutral tripodal vanadium complexes exhibit superior efficiency across various crucial steps of the NRR compared to the Schrock's vanadium catalyst. In view of the lack of comprehensive studies on the NRR catalyzed by vanadium complexes (compared to extensively studied Mo or Fe catalysis), we hope that our present work will help in better understanding of the vanadium-mediated NRR process, and inspire synthetic chemists to pursue the chemistry of tripodal vanadium complexes.

Author contributions

A. K. P. conceived, designed, and supervised the project. B. G. performed the computational studies and S. A. helped with finalization of the manuscript. A. K. P. and B. G. wrote the manuscript. All authors contributed to the discussion of the results and finalization of the manuscript.

Data availability

Tables containing different calculated geometrical and electronic parameters, important molecular orbitals and Cartesian coordinates (in Angstrom) of all the molecules along with their total energies (in Hartree) including zero point vibrational correction.

This information is available free of charge at the website: <https://pubs.rsc.org>.

The data supporting this article have been included as part of the ESI.†

Conflicts of interest

The authors declare no competing financial interest.

Acknowledgements

A. K. P. thanks the Department of Science and Technology (DST-SERB), New Delhi, for providing financial assistance in the form of a research project (project no. CRG/2020/004775). B. G. thanks UGC for the NFOBC fellowship.

References

- J. E. Huheey, E. A. Keiter and R. L. Keiter, *Inorganic Chemistry: Principles of Structure and Reactivity*, Harper Collins College Publishers, New York, 1993.
- J. R. Jennings, *Catalytic Ammonia Synthesis: Fundamentals and Practice*, ed. and J. R. Jennings, Springer Science & Business Media, 1991.
- R. Schlögl, Ammonia Synthesis, in *Handbook of Heterogeneous Catalysis*, Wiley-VCH, 2008, pp. 2501–2575.
- B. M. Hoffman, D. Lukoyanov, Z.-Y. Yang, D. R. Dean and L. C. Seefeldt, *Chem. Rev.*, 2014, **114**, 4041–4062.
- J. Kirn and D. Rees, *Nature*, 1992, **360**, 553–560.
- K. M. Lancaster, M. Roemelt, P. Ettenhuber, Y. Hu, M. W. Ribbe, F. Neese, U. Bergmann and S. DeBeer, *Science*, 2011, **334**, 974–977.
- M. J. Chalkley, M. W. Drover and J. C. Peters, *Chem. Rev.*, 2020, **120**, 5582–5636.
- M. G. Scheibel and S. Schneider, *Angew. Chem., Int. Ed.*, 2012, **51**, 4529–4531.
- Y. Tanabe and Y. Nishibayashi, *Chem. Soc. Rev.*, 2021, **50**, 5201–5242.
- Y. Nishibayashi, *Dalton Trans.*, 2018, **47**, 11290–11297.
- D. V. Yandulov and R. R. Schrock, *Science*, 2003, **301**, 76–78.
- R. R. Schrock, *Angew. Chem., Int. Ed.*, 2008, **47**, 5512–5522.
- D. V. Yandulov and R. R. Schrock, *Inorg. Chem.*, 2005, **44**, 1103–1117.
- R. R. Schrock, *Acc. Chem. Res.*, 2005, **38**, 955–962.
- F. Studt and F. Tuzcek, *Angew. Chem., Int. Ed.*, 2005, **44**, 5639–5642.
- M. Reiher, B. Le Guennic and B. Kirchner, *Inorg. Chem.*, 2005, **44**, 9640–9642.
- S. Schenk, B. Le Guennic, B. Kirchner and M. Reiher, *Inorg. Chem.*, 2008, **47**, 3634–3650.
- S. Schenk, B. Kirchner and M. Reiher, *Chem. – Eur. J.*, 2009, **15**, 5073–5082.
- (a) W. Thimm, C. Gradert, H. Broda, F. Wennmohs, F. Neese and F. Tuzcek, *Inorg. Chem.*, 2015, **54**, 9248–9255; (b) Z. Benedek, M. Papp, J. Oláh and T. Szilvási, *Inorg. Chem.*, 2018, **57**, 8499–8508.
- K. Arashiba, Y. Miyake and Y. Nishibayashi, *Nat. Chem.*, 2011, **3**, 120–125.
- A. Eizawa, K. Arashiba, H. Tanaka, S. Kuriyama, Y. Matsuo, K. Nakajima, K. Yoshizawa and Y. Nishibayashi, *Nat. Commun.*, 2017, **8**, 1–12.
- J. S. Anderson, J. Rittle and J. C. Peters, *Nature*, 2013, **501**, 84–87.
- T. J. Del Castillo, N. B. Thompson and J. C. Peters, *J. Am. Chem. Soc.*, 2016, **138**, 5341–5350.
- N. P. Mankad, M. T. Whited and J. C. Peters, *Angew. Chem., Int. Ed.*, 2007, **46**, 5768–5771.
- Y. Lee, N. P. Mankad and J. C. Peters, *Nat. Chem.*, 2010, **2**, 558–565.
- N. Stucke, B. M. Flöser, T. Weyrich and F. Tuzcek, *Eur. J. Inorg. Chem.*, 2018, **2018**, 1337–1355.
- G. Ung and J. C. Peters, *Angew. Chem., Int. Ed.*, 2015, **54**, 532–535.
- S. Kuriyama and Y. Nishibayashi, *Tetrahedron*, 2021, **83**, 131986.
- F. Masero, M. A. Perrin, S. Dey and V. Mougel, *Chem. – Eur. J.*, 2021, **27**, 3892–3928.
- J. Fajardo Jr. and J. C. Peters, *J. Am. Chem. Soc.*, 2017, **139**, 16105–16108.
- S. Kuriyama, K. Arashiba, H. Tanaka, Y. Matsuo, K. Nakajima, K. Yoshizawa and Y. Nishibayashi, *Angew. Chem., Int. Ed.*, 2016, **55**, 14291–14295.
- N. C. Smythe, R. R. Schrock, P. Müller and W. W. Weare, *Inorg. Chem.*, 2006, **45**, 9197–9205.
- A. K. Guha and A. K. Phukan, *Inorg. Chem.*, 2011, **50**, 8826–8833.
- Y. Sekiguchi, K. Arashiba, H. Tanaka, A. Eizawa, K. Nakajima, K. Yoshizawa and Y. Nishibayashi, *Angew. Chem., Int. Ed.*, 2018, **57**, 9064–9068.
- Y. Kokubo, C. Yamamoto, K. Tsuzuki, T. Nagai, A. Katayama, T. Ohta, T. Ogura, Y. Wasada-Tsutsui, Y. Kajita and S. Kugimiya, *Inorg. Chem.*, 2018, **57**, 11884–11894.
- Y. Kokubo, Y. Wasada-Tsutsui, S. Yomura, S. Yanagisawa, M. Kubo, S. Kugimiya, Y. Kajita, T. Ozawa and H. Masuda, *Eur. J. Inorg. Chem.*, 2020, **2020**, 1456–1464.
- W. Huang, L.-Y. Peng, J. Zhang, C. Liu, G. Song, J.-H. Su, W.-H. Fang, G. Cui and S. Hu, *J. Am. Chem. Soc.*, 2023, **145**, 811–821.
- Y. Tanabe and Y. Nishibayashi, *Coord. Chem. Rev.*, 2019, **381**, 135–150.
- In our study, we have considered only the bare vanadium complex (i.e., without the attached solvent molecule, THF). Furthermore, in order to reduce the computational cost, the HIPT groups attached to the N atom were replaced with phenyl groups.
- Y. Zhao and D. G. Truhlar, *J. Chem. Phys.*, 2006, **125**, 194101.
- M. M. Francl, W. J. Pietro, W. J. Hehre, J. S. Binkley, M. S. Gordon, D. J. DeFrees and J. A. Pople, *J. Chem. Phys.*, 1982, **77**, 3654–3665.
- V. A. Rassolov, J. A. Pople, M. A. Ratner and T. L. Windus, *J. Chem. Phys.*, 1998, **109**, 1223–1229.
- V. A. Rassolov, M. A. Ratner, J. A. Pople, P. C. Redfern and L. A. Curtiss, *J. Comput. Chem.*, 2001, **22**, 976–984.

- 44 D. G. Gusev, *Organometallics*, 2013, **32**, 4239–4243.
- 45 L. S. Yamout, M. Ataya, F. Hasanayn, P. L. Holland, A. J. Miller and A. S. Goldman, *J. Am. Chem. Soc.*, 2021, **143**, 9744–9757.
- 46 B. B. Averkiev and D. G. Truhlar, *Catal. Sci. Technol.*, 2011, **1**, 1526–1529.
- 47 A. A. Chamkin and E. S. Serkova, *J. Comput. Chem.*, 2020, **41**, 2388–2397.
- 48 N. X. Gu, P. H. Oyala and J. C. Peters, *Angew. Chem., Int. Ed.*, 2021, **60**, 4009–4013.
- 49 N. X. Gu, P. H. Oyala and J. C. Peters, *J. Am. Chem. Soc.*, 2020, **142**, 7827–7835.
- 50 R. K. Raju, A. A. Bengali and E. N. Brothers, *Dalton Trans.*, 2016, **45**, 13766–13778.
- 51 B. J. Graziano, M. V. Vollmer and C. C. Lu, *Angew. Chem., Int. Ed.*, 2021, **60**, 15087–15094.
- 52 R. C. Cammarota, J. Xie, S. A. Burgess, M. V. Vollmer, K. D. Vogiatzis, J. Ye, J. C. Linehan, A. M. Appel, C. Hoffmann and X. Wang, *Chem. Sci.*, 2019, **10**, 7029–7042.
- 53 M. E. Moret and J. C. Peters, *Angew. Chem., Int. Ed.*, 2011, **50**, 2063–2067.
- 54 J. S. Anderson, G. E. Cutsail III, J. Rittle, B. A. Connor, W. A. Gunderson, L. Zhang, B. M. Hoffman and J. C. Peters, *J. Am. Chem. Soc.*, 2015, **137**, 7803–7809.
- 55 M. Cossi, G. Scalmani, N. Rega and V. Barone, *J. Chem. Phys.*, 2002, **117**, 43–54.
- 56 S. Grimme, J. Antony, S. Ehrlich and H. Krieg, *J. Chem. Phys.*, 2010, **132**, 154104.
- 57 E. D. Glendening, A. E. Reed, J. E. Carpenter and F. Weinhold, *NBO, version 3.1*, University of Wisconsin, Madison, WI, 1988.
- 58 M. J. Frisch, G. W. Trucks, H. B. Schlegel, G. E. Scuseria, M. A. Robb, J. R. Cheeseman, G. Scalmani, V. Barone, B. Mennucci, G. A. Petersson, H. Nakatsuji, M. Caricato, X. Li, H. P. Hratchian, A. F. Izmaylov, J. Bloino, G. Zheng, J. L. Sonnenberg, M. Hada, M. Ehara, K. Toyota, R. Fukuda, J. Hasegawa, M. Ishida, T. Nakajima, Y. Honda, O. Kitao, H. Nakai, T. Vreven, J. A. Montgomery Jr., J. E. Peralta, F. Ogliaro, M. Bearpark, J. J. Heyd, E. Brothers, K. N. Kudin, V. N. Staroverov, R. Kobayashi, J. Normand, K. Raghavachari, A. Rendell, J. C. Burant, S. S. Iyengar, J. Tomasi, M. Cossi, N. Rega, J. M. Millam, M. Klene, J. E. Knox, J. B. Cross, V. Bakken, C. Adamo, J. Jaramillo, R. Gomperts, R. E. Stratmann, O. Yazyev, A. J. Austin, R. Cammi, C. Pomelli, J. W. Ochterski, R. L. Martin, K. Morokuma, V. G. Zakrzewski, G. A. Voth, P. Salvador, J. J. Dannenberg, S. Dapprich, A. D. Daniels, Ö. Farkas, J. B. Foresman, J. V. Ortiz, J. Cioslowski and D. J. Fox, *Gaussian 09, revision D.01*, Gaussian, Inc., Wallingford, CT, 2009.
- 59 Z. Benedek, M. Papp, J. Oláh and T. Szilvási, *Inorg. Chem.*, 2019, **58**, 7969–7977.
- 60 J. Junge, T. A. Engesser and F. Tuczek, *Chem. – Eur. J.*, 2022, **58**, e202202629.
- 61 Y. Zhao and D. G. Truhlar, *Theor. Chem. Acc.*, 2008, **120**, 215–241.
- 62 F. Weigend and R. Ahlrichs, *Phys. Chem. Chem. Phys.*, 2005, **7**, 3297–3305.
- 63 F. Weigend, *Phys. Chem. Chem. Phys.*, 2006, **8**, 1057–1065.
- 64 C. Adamo and V. Barone, *J. Chem. Phys.*, 1999, **110**, 6158–6170.
- 65 A. Becke, *J. Chem. Phys.*, 1993, **98**, 5648–5652.
- 66 J. Rittle and J. C. Peters, *J. Am. Chem. Soc.*, 2017, **139**, 3161–3170.
- 67 U. Gogoi, A. K. Guha and A. K. Phukan, *Chem. – Eur. J.*, 2013, **19**, 11077–11089.
- 68 M. J. Chalkley, T. J. Del Castillo, B. D. Matson, J. P. Roddy and J. C. Peters, *ACS Cent. Sci.*, 2017, **3**, 217–223.
- 69 P. J. Hill, L. R. Doyle, A. D. Crawford, W. K. Myers and A. E. Ashley, *J. Am. Chem. Soc.*, 2016, **138**, 13521–13524.
- 70 B. M. Barney, D. Lukoyanov, T.-C. Yang, D. R. Dean, B. M. Hoffman and L. C. Seefeldt, *Proc. Natl. Acad. Sci. U. S. A.*, 2006, **103**, 17113–17118.
- 71 N. B. Thompson, M. T. Green and J. C. Peters, *J. Am. Chem. Soc.*, 2017, **139**, 15312–15315.
- 72 J. Rittle and J. C. Peters, *J. Am. Chem. Soc.*, 2016, **138**, 4243–4248.
- 73 E. A. Boyd and J. C. Peters, *J. Am. Chem. Soc.*, 2023, **145**, 14784–14792.
- 74 P. Garrido-Barros, M. J. Chalkley and J. C. Peters, *Angew. Chem., Int. Ed.*, 2023, **62**, e202216693.
- 75 S. Kuriyama, K. Arashiba, K. Nakajima, Y. Matsuo, H. Tanaka, K. Ishii, K. Yoshizawa and Y. Nishibayashi, *Nat. Commun.*, 2016, **7**, 12181.
- 76 J. Fajardo Jr and J. C. Peters, *Inorg. Chem.*, 2021, **60**, 1220–1227.
- 77 S. E. Creutz and J. C. Peters, *J. Am. Chem. Soc.*, 2014, **136**, 1105–1115.